PERGAMON

International Journal of Solids and Structures 40 (2003) 951–980

INTERNATIONAL JOURNAL OF SOLIDS and STRUCTURES

www.elsevier.com/locate/ijsolstr

Meso-macro modelling of fibre-reinforced rubber-like composites exhibiting large elastoplastic deformation

Stefanie Reese *

Department of Civil Engineering, Institute for Mechanics, Ruhr University Bochum, Gebaude IA, Raum 01.128, D-44780 Bochum, Germany

Received 20 October 2001; received in revised form 23 September 2002

Abstract

Many composites consist of a fabric structure embedded in a matrix material. As an example, in the present paper, the case of pneumatic membranes is considered. Fibres are often made of material which shows noticeable plastic deformation. The stiffness of the fibres determines the overall stiffness of the material such that the correct modelling of the orthotropy of the composite is very important. In addition, the structure experiences large deformations which must be accounted for. Suitable models for this type of materials are therefore derived in the framework of finite anisotropic plasticity. A main problem is, however, the lack of experimental data in the literature. For this reason, a computer model of the composite is set up for numerical experiments. In this way, sufficient data can be generated. The present continuum mechanical model based on these "artificial" test data can be efficiently implemented into a finite element formulation. Using a special integration algorithm, the non-linear equation system consisting initially of 10 equations reduces to two non-linear scalar equations.

Keywords: Orthotropic material behaviour; Fabric structure; Pneumatic membrane; Finite elements; Virtual testing; Anisotropy; Parameter identification

1. Introduction

Many fibre-reinforced composites consist of a fabric structure embedded in a matrix material. In the case of pneumatic membranes, the fibres are made of polyester, glass aramide or carbon fibres which have been shown experimentally to exhibit noticeable plastic deformation. Common matrix materials are rubber, PVC or Teflon. A realistic mathematical description of the material behaviour of the composite can only be achieved if a sufficient number of experiments is carried out. Due to the anisotropy of the material, this is

* Tel.: +49-234-32-25883; fax: +49-234-32-14488.
E-mail address: reese@nm.ruhr-uni-bochum.de (S. Reese).

0020-7683/02/$ - see front matter
PII: S0020-7683(02)00602-9

hardly possible in practice, since there are not enough experimental results available in the literature in order to validate a new material model. To circumvent this difficulty, we begin here the material modelling on the meso-scale. Using a so-called computer model, we generate artificial experimental data. The computer simulation firstly serves to understand the special deformation behaviour of the composite material. On the other hand, the data are used to derive a physically reasonable continuum mechanical model of finite anisotropic elastoplasticity.

Anisotropic elastoplasticity has up to now mainly attracted attention in the context of crystal plasticity, where the structural vectors in the intermediate configuration are fixed and the yield condition is formulated in terms of the Schmidt stress. Refer for example to the classical works of Hill (1966), Rice (1971) and Asaro (1983). For the computational aspects see Cuitino and Ortiz (1992) and Miehe (1996). In the present work, the situation is different in the regard that the fibre orientations represent so-called material directions. The structural vectors transform like material line elements. In the following, this kind of material behaviour will be described in the framework of *phenomenological* anisotropic modelling (in contrast to crystal plasticity, where micromechanical effects are taken into account). To the knowledge of the author, a concrete model for such kind of anisotropic elastoplasticity has not yet been published in the literature. In the context of pneumatic membranes, it has to be additionally taken into account that the fibres carry load *only* in tension.

In the field of phenomenological anisotropic material modelling at finite strains, several papers focus on biomechanical problems (Holzapfel et al., 1996, 2000; Weiss et al., 1996; Bonet and Burton, 1998; Gasser and Holzapfel, submitted for publication). Among the latter authors, only Gasser and Holzapfel (submitted for publication) include anisotropic elasto*plasticity*. An alternative approach for fabric-reinforced composites can be found in the recent work of Spencer (2001). Other new formulations of anisotropic material behaviour have been proposed by Menzel and Steinmann (2001), Sansour and Kollmann (2001) and Schmidt (2001). The work of Reese et al. (2001) includes one of the few models for the large deformation behaviour of pneumatic membranes. This concept is, however, restricted to purely *elastic* material behaviour.

The present model is developed in three steps. Firstly (step I), experimental results available for the polyester fibres are exploited to determine the material parameters of a one-dimensional (1D) incompressible elastoplastic 1D model. The latter is inserted into the computer model, where the fibres are modelled by means of truss elements. The rubber coating is represented by continuum elements. Using such a detailed discretization on the meso-scale, one is able to simulate experimental tests. Note that (computer) test data could also be obtained via a numerical homogenization procedure as it is common in the context of crystal plasticity or metallic composites. But due to the non-linearity of the meso-stress–strain relationships, it is in neither case possible to derive an *analytical* macromechanical stress–strain relation. Thus, if one is interested to model the material behaviour phenomenologically, a continuum mechanical model has to be additionally constructed upon the characteristics of the "test" data (step II).

The present model is based on the idea that plastification occurs, if a certain limit stress in the fibre is exceeded. It is a highly challenging task to show the consistency of such a model with the dissipation inequality. A surprising result is the fact that the plastic deformation is represented by a symmetric tensor-valued variable. In fact, this can be shown to be the case for more general kinds of anisotropy based on symmetric structural tensors (see also Svendsen and Reese, submitted for publication). Thus, as in isotropic elastoplasticity, the plastic spin remains undetermined.

The latter observation proves to be advantageous also from the numerical point of view. The number of unknowns at the Gauss point level is noticeably reduced. In addition, by means of a suitable integration procedure the system of originally 10 non-linear equations boils down to two non-linear equations and eight functional evaluations. The model can therefore easily be incorporated into a finite element formulation (step III).

2. Computer model

2.1. Fibres

Fig. 1 shows "real" experimental results (uniaxial tension) for the two fibre directions of the fabric (polyester threads). The stiffer thread is called warp thread, the other one-weft thread. The strain values are given in percent and refer to the linearized strain measure $\Delta L/L$ (L initial length of the test sample). One observes a noticeable permanent deformation, when unloading takes place. Note that the hysteresis visible during reloading is not shown in the picture. In other words, we neglect the rate-dependence of the material behaviour which is, however, rather small.

The material behaviour of the fibres seems to be somewhat rubber-like. This suggests a model which is usually applied in the context of rubber elasticity (see Ogden, 1984). The extension to elastoplasticity is straightforward (Table 1). In these equations, σ denotes the Cauchy stress and λ the stretch along the fibre axis. It is multiplicatively decomposed into elastic (λ_e) and plastic (λ_p) parts. Using the assumption of incompressibility, σ can be directly computed from the force F and the initial cross-sectional area A. The yield criterion is standard besides the non-linear isotropic hardening term $H_{nl}\xi^{\chi}$ (ξ accumulated plastic strain). The quantity $\dot{\gamma}$ represents the plastic multiplier. The material parameters used for the fit in Fig. 1 are given below:

$$\begin{aligned} \text{warp thread}: \quad & \mu = 195.95 \quad \mathrm{N/mm^2}, \qquad \alpha = 30.37, \qquad \sigma_{Y0} = 111.5 \quad \mathrm{N/mm^2}, \\ & H_{\mathrm{lin}} = 5969.49 \quad \mathrm{N/mm^2}, \qquad H_{\mathrm{nl}} = 43977191 \quad \mathrm{N/mm^2}, \qquad \chi = 4.37; \end{aligned} \tag{1}$$

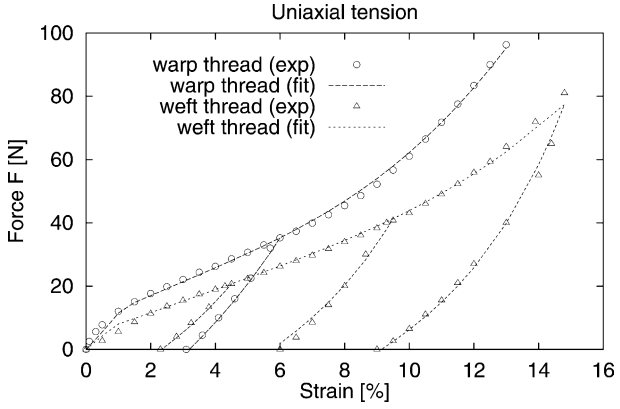

Fig. 1. Experimental results and fit for uniaxial tension.

Table 1
Constitutive model of 1D elastoplasticity

Elastic material law	$\sigma = \mu(\lambda_e^{\alpha} - \lambda_e^{-0.5\alpha})$, $F = \sigma\frac{A}{\lambda}$
Stretch	$\lambda = 1 + \frac{\varepsilon(\%)}{100} = \lambda_e\lambda_p$
Yield condition	$\Phi = \lvert\sigma\rvert - (\sigma_{Y0} + H_{\mathrm{lin}}\xi + H_{\mathrm{nl}}\xi^{\chi}) \leqslant 0$
Flow rules	$\dot{\lambda}_p = \dot{\gamma}\,\mathrm{sign}\,\sigma\lambda_p$, $\dot{\xi} = \dot{\gamma}$ with $\Phi \leqslant 0$, $\dot{\gamma}\Phi = 0$, $\dot{\gamma} \geqslant 0$

$$\begin{aligned} \text{weft thread}: \quad & \mu = 121.79 \quad \mathrm{N/mm^2}, \qquad \alpha = 36.95, \qquad \sigma_{Y0} = 62.95 \quad \mathrm{N/mm^2}, \\ & H_{\mathrm{lin}} = 5051.48 \quad \mathrm{N/mm^2}, \qquad H_{\mathrm{nl}} = 12738581 \quad \mathrm{N/mm^2}, \qquad \chi = 4.47. \end{aligned} \tag{2}$$

For a common rubber material, the parameter α would take on values around 2. In the present case, however, the characteristic S-shape of the force–strain curve appears in the small strain range. For this reason, the value of α is here much higher.

2.2. Composite

Experimental data for composites are frequently found in the form of internal reports of companies but are poorly documented in the available literature. In order to overcome this problem, we set up a "computer testing device" to obtain appropriate stress–strain data. The material parameters of the orthotropic continuum mechanical model will then be fitted to these "experimental" results (Section 3).

In Fig. 2, the computer model for the fibre-reinforced membrane is shown. It consists of 3D non-linear truss elements modeling the fibres and special low-order brick elements describing the rubber coating.

To get a representative response, 10 (to be precise nine in the interior and two cut in half at the boundary) fibres are placed in each direction. With this two-phase approach, one is able to model the two constituents separately. For the rubber, the standard Neo–Hookean approach is used. The material behaviour of the polyester fibres is described by means of the model derived in Section 2.1.

Since the fibres are not fully extended in their initial configuration (solid line in Fig. 3), one can pull them in a stress-free state up to the point, where they are stretched straight. The strain at this time is easily calculated from comparing the initial length of the fibres ($L = 10.44$ mm) with the length of the test sample (10 mm). So, the stresses measured up to a strain of about $\Delta L/L = 0.44/10 = 4.4\%$ are due to the influence of the rubber matrix alone and therefore very small (see the rubber elastic range in Fig. 5). The complete stress–strain plot is given in Fig. 4. Beyond this limit, the stress in the fibres increases rapidly and the stress–strain relationship of the membrane is dominated by the behaviour of the fibres (anisotropic elastic range).

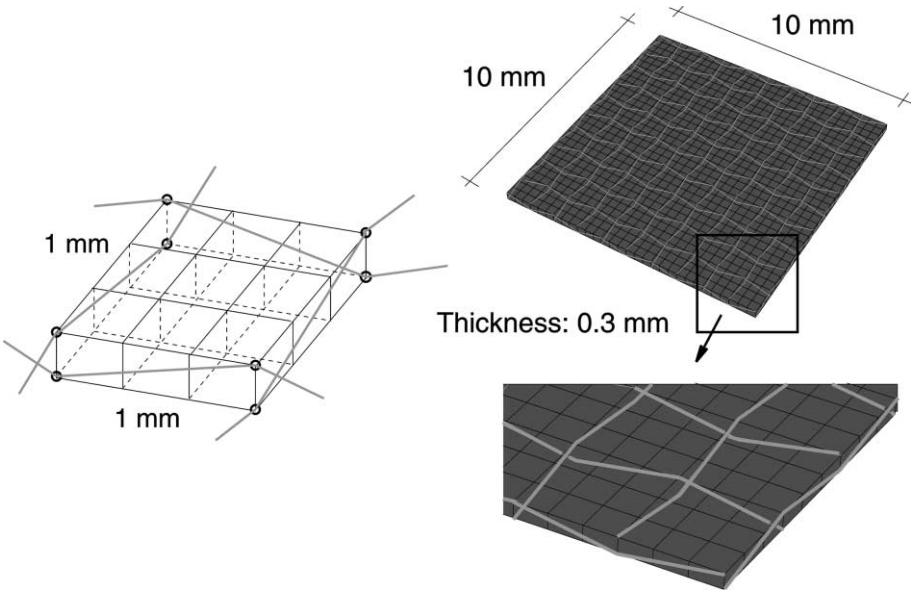

Fig. 2. Computer model.

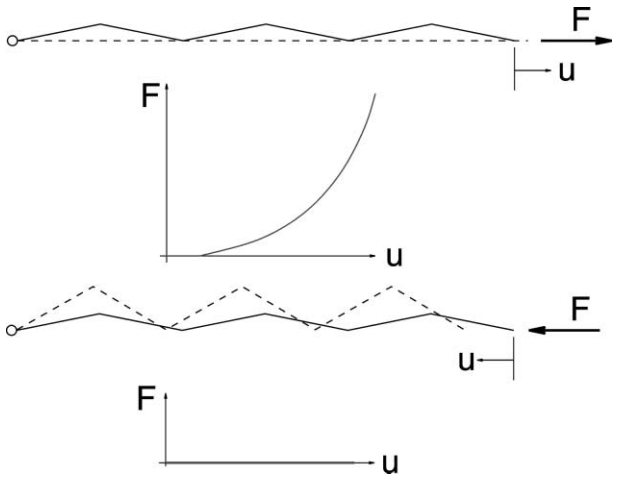

Fig. 3. Fibre behaviour under tension and compression.

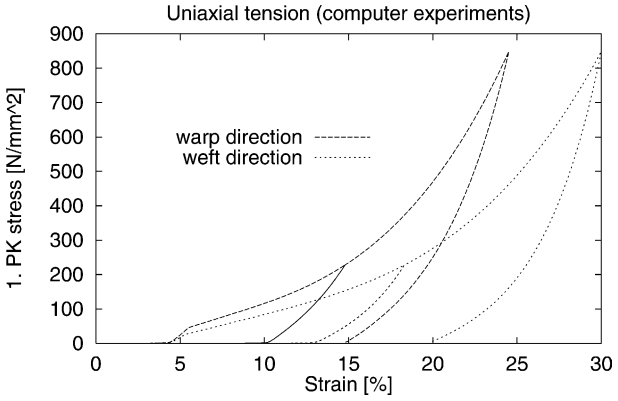

Fig. 4. Computer experiments.

The yield point is indicated by the kink in Fig. 5. The threads are permanently lengthened by the evolution of the plastic strain. Thus, on the unloading path, they return to the stress-free state already at a strain of about 10% (warp thread) or 13% (weft thread), respectively. From this point on, the load is carried again only by the rubber coating. So, although there is a permanent deformation in the fibres, the deformation of the "computer" membrane is completely reversible. In the direction of compression, the situation is in general similar to the small strain case.

3. Continuum model

3.1. Strain energy function

We describe the deformation of a continuous body by means of the right Cauchy–Green tensor

$$\mathbf{C} = \mathbf{F}^{\mathrm{T}} \cdot \mathbf{F}, \tag{3}$$

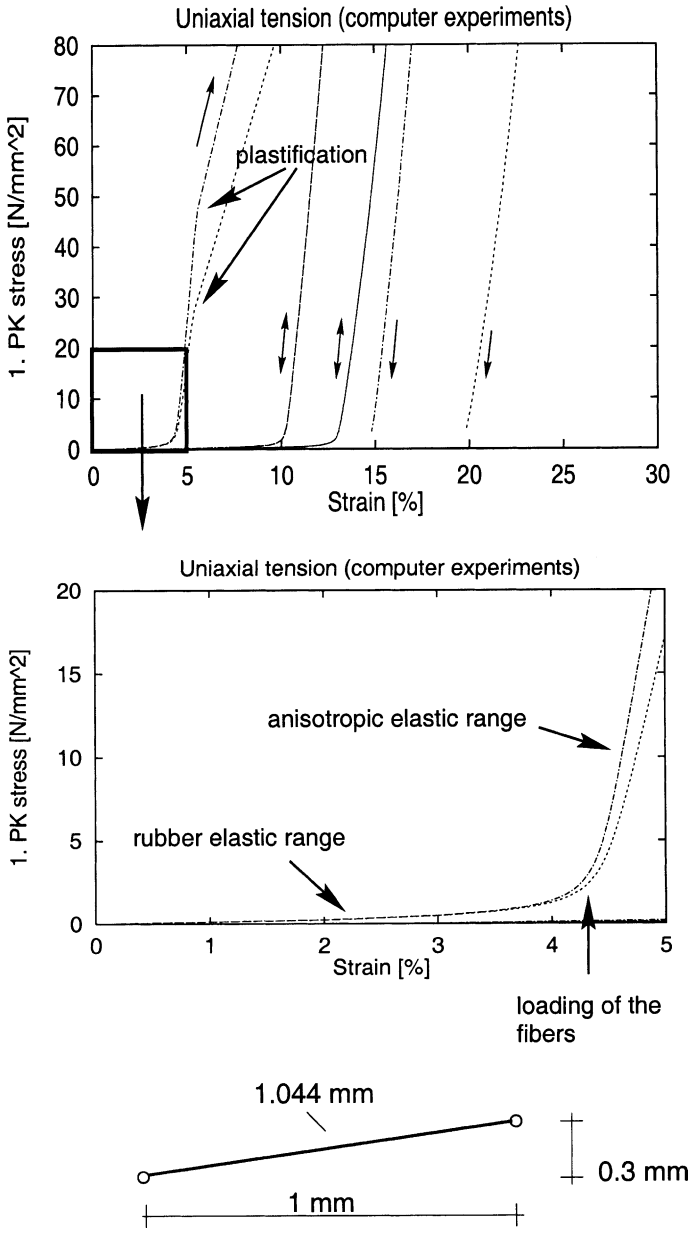

Fig. 5. Detail of Fig. 4.

where $\mathbf{F}$ denotes the deformation gradient. We assume further the existence of a scalar potential $\Psi = W(\mathbf{C}, \mathbf{F}_p) + f(\boldsymbol{\varepsilon})$ (Helmholtz free energy function per reference volume), where $\mathbf{F}_p$ represents the plastic part of the deformation gradient. The vector $\boldsymbol{\varepsilon}$ contains certain internal variables which are specified later in the context of the model. The part $W(\mathbf{C}, \mathbf{F}_p)$ is usually called strain energy function. If $\mathbf{F}_p$ is considered as elastic isomorphism (Wang and Bloom, 1974; Bertram, 1992, 1998; Svendsen, 1998), W can be represented as a function of the "elastic" right Cauchy–Green tensor $\mathbf{C}_e = \mathbf{F}_p^{-T} \cdot \mathbf{C} \cdot \mathbf{F}_p^{-1} = \mathbf{F}_e^T \cdot \mathbf{F}_e$, the elastic part of the

deformation gradient defined by $\mathbf{F}_e = \mathbf{F} \cdot \mathbf{F}_p^{-1}$. To model orthotropic material behaviour, the strain energy function is represented as an isotropic function of $\mathbf{C}_e$ and the structural tensors

$$\widetilde{\mathbf{M}}_1 = \widetilde{\mathbf{N}}_1 \otimes \widetilde{\mathbf{N}}_1, \qquad \widetilde{\mathbf{M}}_2 = \widetilde{\mathbf{N}}_2 \otimes \widetilde{\mathbf{N}}_2. \tag{4}$$

Thus, it can be written in the form

$$W = W_{\text{isotr}}\left(\mathbf{F}_p^{-T} \cdot \mathbf{C} \cdot \mathbf{F}_p^{-1}, \widetilde{\mathbf{M}}_1, \widetilde{\mathbf{M}}_2\right), \tag{5}$$

where the index "isotr" indicates here that W is an isotropic function of the given quantities. See for a more detailed discussion the theoretical works of Boehler (1977, 1979), Liu (1982), Zhang and Rychlewski (1990) and Svendsen (1994, 2001). It is important to note that $\mathbf{C}_e$, $\widetilde{\mathbf{M}}_1$, and $\widetilde{\mathbf{M}}_2$ are tensors in the intermediate configuration. The vectors $\widetilde{\mathbf{N}}_i$ $(i = 1, 2)$ are given via the equation $(i = 1, 2)$

$$\widetilde{\mathbf{N}}_i = \mathbf{F}_p \cdot \mathbf{N}_i \frac{1}{|\mathbf{F}_p \cdot \mathbf{N}_i|} \Rightarrow \widetilde{\mathbf{M}}_i = \mathbf{F}_p \cdot \mathbf{M}_i \cdot \mathbf{F}_p^T \frac{1}{\mathbf{C}_p : \mathbf{M}_i} \quad \text{with } \mathbf{M}_i = \mathbf{N}_i \otimes \mathbf{N}_i, \tag{6}$$

where the vectors $\mathbf{N}_i$ are oriented parallel to the fibres in the *reference* configuration (see Fig. 6).

Analogously, we define the structural tensors $\mathbf{m}_i$ with respect to the current configuration by means of

$$\mathbf{m}_i = \mathbf{n}_i \otimes \mathbf{n}_i = \mathbf{F}_e \cdot \widetilde{\mathbf{M}}_i \cdot \mathbf{F}_e^T \frac{1}{\mathbf{C}_e : \widetilde{\mathbf{M}}_i} \quad \text{with } \mathbf{n}_i = \mathbf{F}_e \cdot \widetilde{\mathbf{N}}_i \frac{1}{|\mathbf{F}_e \cdot \widetilde{\mathbf{N}}_i|}. \tag{7}$$

Note that in general

$$\widetilde{\mathbf{N}}_1 \cdot \widetilde{\mathbf{N}}_2 \neq 0, \qquad \mathbf{n}_1 \cdot \mathbf{n}_2 \neq 0 \tag{8}$$

holds, i.e. the material is only initially orthotropic ($\mathbf{N}_1 \cdot \mathbf{N}_2 = 0$). The fibres do not remain orthogonal to each other.

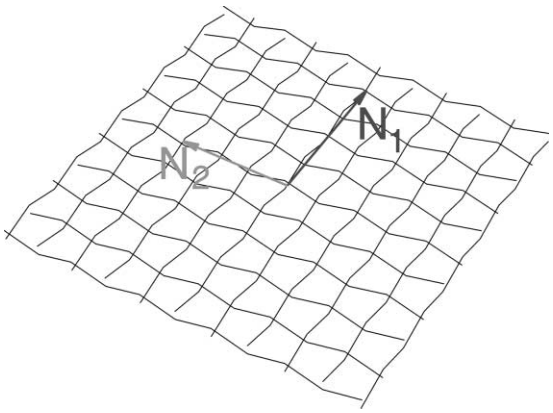

Fig. 6. Roven–woven structure with vectors $\mathbf{N}_i$ $(i = 1, 2)$.

The strain energy function $W_{\text{isotr}}(\mathbf{C}_e, \widetilde{\mathbf{M}}_1, \widetilde{\mathbf{M}}_2)$ can be formulated in terms of the three invariants of $\mathbf{C}_e$,2

$$I_1 := \operatorname{tr}\mathbf{C}_e, \qquad I_2 := \tfrac{1}{2}\big(I_1^2 - \operatorname{tr}(\mathbf{C}_e^2)\big), \qquad I_3 := \det \mathbf{C}_e \tag{9}$$

and the first invariants of $\mathbf{C}_e \cdot \widetilde{\mathbf{M}}_1$, $\mathbf{C}_e^2 \cdot \widetilde{\mathbf{M}}_1$, $\mathbf{C}_e \cdot \widetilde{\mathbf{M}}_2$, $\mathbf{C}_e^2 \cdot \widetilde{\mathbf{M}}_2$, $\widetilde{\mathbf{M}}_1 \cdot \widetilde{\mathbf{M}}_2$ and $\mathbf{C}_e \cdot \widetilde{\mathbf{M}}_1 \cdot \widetilde{\mathbf{M}}_2$, respectively:

$$\begin{aligned} &I_4 := \operatorname{tr}(\mathbf{C}_e \cdot \widetilde{\mathbf{M}}_1) = \mathbf{C}_e : \widetilde{\mathbf{M}}_1, \qquad I_5 := \operatorname{tr}(\mathbf{C}_e^2 \cdot \widetilde{\mathbf{M}}_1) = \mathbf{C}_e^2 : \widetilde{\mathbf{M}}_1, \qquad I_6 := \operatorname{tr}(\mathbf{C}_e \cdot \widetilde{\mathbf{M}}_2) = \mathbf{C}_e : \widetilde{\mathbf{M}}_2, \\ &I_7 := \operatorname{tr}(\mathbf{C}_e^2 \cdot \widetilde{\mathbf{M}}_2) = \mathbf{C}_e^2 : \widetilde{\mathbf{M}}_2, \qquad I_8 := \operatorname{tr}(\widetilde{\mathbf{M}}_1 \cdot \widetilde{\mathbf{M}}_2), \qquad I_9 := \operatorname{tr}(\mathbf{C}_e \cdot \widetilde{\mathbf{M}}_1 \cdot \widetilde{\mathbf{M}}_2). \end{aligned} \tag{10}$$

For simplicity, the dependence on I_8 and I_9 will be neglected. A possible form for the strain energy function is then the following:

$$W = W_{\text{NH}}(I_1, I_3) + W_{+}(I_1, I_2) + W_{\text{ani}}(I_4, I_5, I_6, I_7) \tag{11}$$

$$W_{\text{NH}} = \frac{\mu}{2}(I_1 - 3) - \mu \ln\sqrt{I_3} + \frac{\Lambda}{4}(I_3 - 1 - 2\ln\sqrt{I_3}), \tag{12}$$

$$\begin{aligned} W_{+} &= K_1^{\text{iso}}(I_1 - 3)^{\alpha_1} + K_2^{\text{iso}}(I_2 - 3)^{\alpha_2}, \\ W_{\text{ani}} &= K_1^{\text{ani}\,1}(I_4 - 1)^{\beta_1} + K_2^{\text{ani}\,1}(I_5 - 1)^{\beta_2} + K_1^{\text{ani}\,2}(I_6 - 1)^{\gamma_1} + K_2^{\text{ani}\,2}(I_7 - 1)^{\gamma_2} \\ &\quad + K^{\text{kop}\,1}(I_1 - 3)^{\delta_1}(I_4 - 1)^{\delta_1} + K^{\text{kop}\,2}(I_1 - 3)^{\delta_2}(I_6 - 1)^{\delta_2} + K^{\text{kop}\,12}(I_4 - 1)^{\zeta}(I_6 - 1)^{\zeta}. \end{aligned} \tag{13}$$

The latter form has already been chosen by Reese et al. (2001), where only hyperelastic material behaviour was considered. In contrast to this earlier work, here, the invariants I_j ($j = 1, \ldots, 7$) are computed in terms of $\mathbf{C}_e$ and $\widetilde{\mathbf{M}}_i$ ($i = 1, 2$). In hyperelasticity, $\mathbf{C}_e$ reduces to $\mathbf{C}$ and $\widetilde{\mathbf{M}}_i$ to $\mathbf{M}_i$. The Neo–Hooke part W_{NH} models the deformation behaviour of the rubber coating. In the rubber elastic range, this represents the dominating part in the strain energy function. Consider now a deformation with $(C_e)_{11} > 1$, $(C_e)_{22} < 1$, $(C_e)_{33} = (C_e)_{11}^{-1}(C_e)_{22}^{-1}$ and $(C_e)_{ij} = 0$, if $i \neq j$. The vectors $\mathbf{N}_i$ ($i = 1, 2$) are chosen to be $\mathbf{N}_1^{\text{T}} = \{1, 0, 0\}$ and $\mathbf{N}_2^{\text{T}} = \{0, 1, 0\}$. It is obvious that in such a case, only the fibres in warp direction (index 1) contribute to the stress, since the fibres in weft direction (index 2) are not stretched straight. Then, we observe transversely isotropic material behaviour which can be described with only one structural tensor $\widetilde{\mathbf{M}}_1 = \widetilde{\mathbf{M}}$. The expression $I_4 - 1$ is positive, whereas $I_6 - 1$ is negative. The opposite case is obtained analogously. Compression in warp and weft direction leads to purely isotropic behaviour. These requirements have to be incorporated into the model. For this purpose, the following case differentiation is suitable.

If one of the expressions in the brackets characterized by the structure $\text{inv} - c$ (invariant minus constant) becomes negative (i.e. the fibres in warp or/and weft direction are not stretched straight), the material parameter $K_{\cdots}^{\cdots}$ associated with this term is set equal to zero. In this way, we account for the fact that the fibres do not contribute to the stress in the composite in their relaxed state.

In order to guarantee a smooth transition for $\text{inv} = c$, the exponents α_i, β_i, γ_i, δ_i and ζ ($i = 1, 2$) are not allowed to be equal to 1 or 2. In order to understand the reason for this restriction, we investigate the expression $f(I_4) = (I_4 - 1)^{\beta_1}$ in more detail. Taking the first and the second derivative with respect to $\mathbf{C}$ leads to

$$\frac{\partial f(I_4)}{\partial \mathbf{C}} = \beta_1 (I_4 - 1)^{\beta_1 - 1} \frac{\mathbf{M}_1}{\mathbf{C}_p : \mathbf{M}_1} \tag{14}$$

and

$$\frac{\partial^2 f(I_4)}{\partial \mathbf{C}^2} = (\beta_1 - 1)\beta_1 (I_4 - 1)^{\beta_1 - 2} \frac{\mathbf{M}_1}{\mathbf{C}_p : \mathbf{M}_1} \otimes \frac{\mathbf{M}_1}{\mathbf{C}_p : \mathbf{M}_1}. \tag{15}$$

The term (14) enters the second Piola–Kirchhoff stress tensor $\mathbf{S}$, whereas (15) is part of the material tensor $\mathscr{L} = 4\partial^2 W/\partial \mathbf{C}^2$. The tensor $\mathbf{M}_1/(\mathbf{C}_p : \mathbf{M}_1)$ can be considered to be constant in the following discussion and is therefore (for simplicity) denoted by $\mathbf{Y}$. We then obtain

$$\begin{aligned} &\beta_1 = 1: \quad \frac{\partial f(I_4)}{\partial \mathbf{C}} = \mathbf{Y}, \qquad \frac{\partial^2 f(I_4)}{\partial \mathbf{C}^2} = \mathbf{0}; \\ &\beta_1 = 2: \quad \frac{\partial f(I_4)}{\partial \mathbf{C}} = 2(I_4 - 1)\mathbf{Y}, \qquad \frac{\partial^2 f(I_4)}{\partial \mathbf{C}^2} = 2\mathbf{Y} \otimes \mathbf{Y}. \end{aligned} \tag{16}$$

Thus, if the stiffness $K_1^{\text{ani}\,1}$ is switched off at $I_4 = 1$, either the stress $\mathbf{S}$ ($\beta_1 = 1$) or the material tensor $\mathscr{L}$ ($\beta_1 = 2$) is discontinuous. A smooth transition between different cases (e.g. orthotropy/transversal isotropy) cannot be obtained, if $\beta_1 = 1$ or $\beta_2 = 1$. Similar considerations can be made for the other terms of the strain energy function.

3.2. Dissipation inequality

Using the Helmholtz free energy function $\Psi = W_{\text{isotr}}(\mathbf{F}_p^{-T} \cdot \mathbf{C} \cdot \mathbf{F}_p^{-1}, \widetilde{\mathbf{M}}_1, \widetilde{\mathbf{M}}_2) + f(\boldsymbol{\varepsilon})$ in the Clausius–Duhem form of the second law of thermodynamics leads to the so-called dissipation inequality

$$-\dot{\Psi} + \mathbf{S} : \frac{1}{2}\dot{\mathbf{C}} = \left(\mathbf{S} - 2\frac{\partial W}{\partial \mathbf{C}}\right) : \frac{1}{2}\dot{\mathbf{C}} + \boldsymbol{\Sigma} : \mathbf{l}_p + \mathbf{q} \cdot \dot{\boldsymbol{\varepsilon}} \geqslant 0, \tag{17}$$

where $\mathbf{l}_p$, the stress tensor $\boldsymbol{\Sigma}$ and $\mathbf{q}$ are defined by

$$\mathbf{l}_p := \dot{\mathbf{F}}_p \cdot \mathbf{F}_p^{-1}, \qquad \boldsymbol{\Sigma} = -\frac{\partial W}{\partial \mathbf{F}_p} \cdot \mathbf{F}_p^{T} \quad \text{and} \quad \mathbf{q} = -\frac{\partial f(\boldsymbol{\varepsilon})}{\partial \boldsymbol{\varepsilon}}, \tag{18}$$

respectively. The vector $\boldsymbol{\varepsilon}$ contains internal variables describing the hardening of the material. The inequality (17) is sufficiently fulfilled by $\mathbf{S} = 2\partial W/\partial \mathbf{C}$, $\boldsymbol{\Sigma} : \mathbf{l}_p \geqslant 0$ and $\mathbf{q} \cdot \boldsymbol{\varepsilon} \geqslant 0$. Evidently, there are many possibilities to choose an evolution equation for $\mathbf{l}_p$ in such a way that the latter requirement is satisfied. The main difficulty, however, is to match the "experimental" results.

3.3. Yield functions and flow rules

Using the Gateaux derivative

$$DW(\mathbf{C}_e, \widetilde{\mathbf{M}}_1, \widetilde{\mathbf{M}}_2) : \Delta\mathbf{C} = \frac{\partial W}{\partial \mathbf{C}_e} : (\mathbf{F}_p^{-T} \cdot \Delta\mathbf{C} \cdot \mathbf{F}_p^{-1}), \tag{19}$$

it is easily shown that

$$\mathbf{S} = 2\mathbf{F}_p^{-1} \cdot \frac{\partial W}{\partial \mathbf{C}_e} \cdot \mathbf{F}_p^{-T} \tag{20}$$

holds. From that, we compute the Kirchhoff stress tensor $\boldsymbol{\tau} = \mathbf{F} \cdot \mathbf{S} \cdot \mathbf{F}^{T}$ with (see Appendix A)

$$\begin{aligned}\boldsymbol{\tau} &= 2\mathbf{F}_e \cdot \frac{\partial W}{\partial \mathbf{C}_e} \cdot \mathbf{F}_e^T \\ &= 2\frac{\partial W}{\partial I_1}\mathbf{b}_e + 2\frac{\partial W}{\partial I_2}(I_1\mathbf{b}_e - \mathbf{b}_e^2) + 2\frac{\partial W}{\partial I_3}I_3\mathbf{1} \quad \text{“iso”} \\ &\quad + 2\frac{\partial W}{\partial I_4}\overline{\mathbf{m}}_1 + 2\frac{\partial W}{\partial I_5}(\mathbf{b}_e \cdot \overline{\mathbf{m}}_1 + \overline{\mathbf{m}}_1 \cdot \mathbf{b}_e) \quad \text{“ani 1”} \\ &\quad + 2\frac{\partial W}{\partial I_6}\overline{\mathbf{m}}_2 + 2\frac{\partial W}{\partial I_7}(\mathbf{b}_e \cdot \overline{\mathbf{m}}_2 + \overline{\mathbf{m}}_2 \cdot \mathbf{b}_e) \quad \text{“ani 2”},\end{aligned} \tag{21}$$

where the tensors $\overline{\mathbf{m}}_i$ $(i = 1, 2)$ are given with $\overline{\mathbf{m}}_i = \mathbf{F}_e \cdot \widetilde{\mathbf{M}}_i \cdot \mathbf{F}_e^T = I_{2i+2}\mathbf{m}_i$. The first three terms (second line of (21)) represent the isotropic part of $\boldsymbol{\tau}$ from now on denoted with $\boldsymbol{\tau}_{iso}$. It is derived from the strain energy parts W_{NH} and W_+ alone. Accordingly, we define $\boldsymbol{\tau}_{ani\,1}$ and $\boldsymbol{\tau}_{ani\,2}$ coming from W_{ani}.

Exploiting the fact that W is an isotropic function of $\mathbf{C}_e$, $\widetilde{\mathbf{M}}_1$ and $\widetilde{\mathbf{M}}_2$, it can be shown that the stress tensor $\boldsymbol{\Sigma}$ is symmetric (see Appendix B):

$$\begin{aligned}\boldsymbol{\Sigma} &= 2\frac{\partial W}{\partial I_1}\mathbf{C}_e + 2\frac{\partial W}{\partial I_2}(I_1\mathbf{C}_e - \mathbf{C}_e^2) + 2\frac{\partial W}{\partial I_3}I_3\mathbf{1} \quad \text{“iso”} \\ &\quad + 2\frac{\partial W}{\partial I_4}I_4\widetilde{\mathbf{M}}_1 + 2\frac{\partial W}{\partial I_5}(I_5\widetilde{\mathbf{M}}_1 + \mathbf{C}_e \cdot \widetilde{\mathbf{M}}_1 \cdot \mathbf{C}_e) \quad \text{“ani 1”} \\ &\quad + 2\frac{\partial W}{\partial I_6}I_6\widetilde{\mathbf{M}}_2 + 2\frac{\partial W}{\partial I_7}(I_7\widetilde{\mathbf{M}}_2 + \mathbf{C}_e \cdot \widetilde{\mathbf{M}}_2 \cdot \mathbf{C}_e) \quad \text{“ani 2”}.\end{aligned} \tag{22}$$

The scalar product $\boldsymbol{\Sigma} : \mathbf{l}_p$ therefore reduces to $\boldsymbol{\Sigma} : \mathbf{d}_p$, where $\mathbf{d}_p = \operatorname{sym}\mathbf{l}_p$ denotes the symmetric part of $\mathbf{l}_p$. The scalar product $\boldsymbol{\Sigma} : \mathbf{d}_p$ can be rewritten with

$$\boldsymbol{\Sigma} : \mathbf{d}_p = \left(\mathbf{F}_p^{-1} \cdot \boldsymbol{\Sigma} \cdot \mathbf{F}_p^{-T}\right) : \tfrac{1}{2}\dot{\mathbf{C}}_p, \tag{23}$$

where the tensor

$$\begin{aligned}\mathbf{F}_p^{-1} \cdot \boldsymbol{\Sigma} \cdot \mathbf{F}_p^{-T} &= 2\mathbf{C}_p^{-1} \cdot \mathbf{C} \cdot \mathbf{S}_{iso}(\mathbf{C}, \mathbf{C}_p) + 2W_{,4}\frac{I_4}{\mathbf{C}_p : \mathbf{M}_1}\mathbf{M}_1 + 2W_{,5}\frac{1}{\mathbf{C}_p : \mathbf{M}_1}\left(I_5\mathbf{M}_1 + \mathbf{C}_p^{-1} \cdot \mathbf{C} \cdot \mathbf{M}_1 \cdot \mathbf{C} \cdot \mathbf{C}_p^{-1}\right) \\ &\quad + 2W_{,6}\frac{I_6}{\mathbf{C}_p : \mathbf{M}_2}\mathbf{M}_2 + 2W_{,6}\frac{1}{\mathbf{C}_p : \mathbf{M}_2}\left(I_7\mathbf{M}_2 + \mathbf{C}_p^{-1} \cdot \mathbf{C} \cdot \mathbf{M}_2 \cdot \mathbf{C} \cdot \mathbf{C}_p^{-1}\right),\end{aligned} \tag{24}$$

obviously represents a function of $\mathbf{C}$ and $\mathbf{C}_p$ (the structural tensors $\mathbf{M}_i$ $(i = 1, 2)$ in the reference configuration can be considered to be given). Therefore, in contrast to many other approaches in anisotropic plasticity, the model is closed if we consider the *symmetric* tensor $\mathbf{C}_p$ as internal variable. The rotational part in $\mathbf{F}_p = \mathbf{R}_p \cdot \sqrt{\mathbf{C}}_p$, i.e. $\mathbf{R}_p$, remains undetermined. The stress tensor $\mathbf{S}_{iso}$ is computed via $\mathbf{S}_{iso} = 2\partial(W_{NH} + W_+)/\partial\mathbf{C} = \mathbf{F}^{-1}\boldsymbol{\tau}_{iso}\mathbf{F}^{-T}$ and represents the isotropic part of $\mathbf{S}$.

At this point, the computer model proves to be very useful, since it enhances our understanding of the material behaviour majorly. The comparison between the stress–strain curves computed for uniaxial and biaxial tension makes evident, that the fibres in warp and weft direction hardly interact with each other (see Fig. 7). This is understandable from the fact that the warp threads are not directly linked to the weft threads (see Fig. 2). The interaction is only due to the rubber matrix, the stiffness of which is very low in comparison with the one of the fibres. So, we are able to treat the pneumatic membrane as two 1D systems which are in its initial state oriented orthogonal to each other. Keeping this in mind, it can be easily accepted that plastification begins, when the Cauchy stress in the fibre direction exceeds a certain value. If one takes additionally into account, that the material is nearly incompressible, we may use instead of the Cauchy stress also the Kirchhoff stress and express the projection of this stress on $\mathbf{n}_i$ in the form $\boldsymbol{\tau} : \mathbf{m}_i$ $(i = 1, 2)$. In

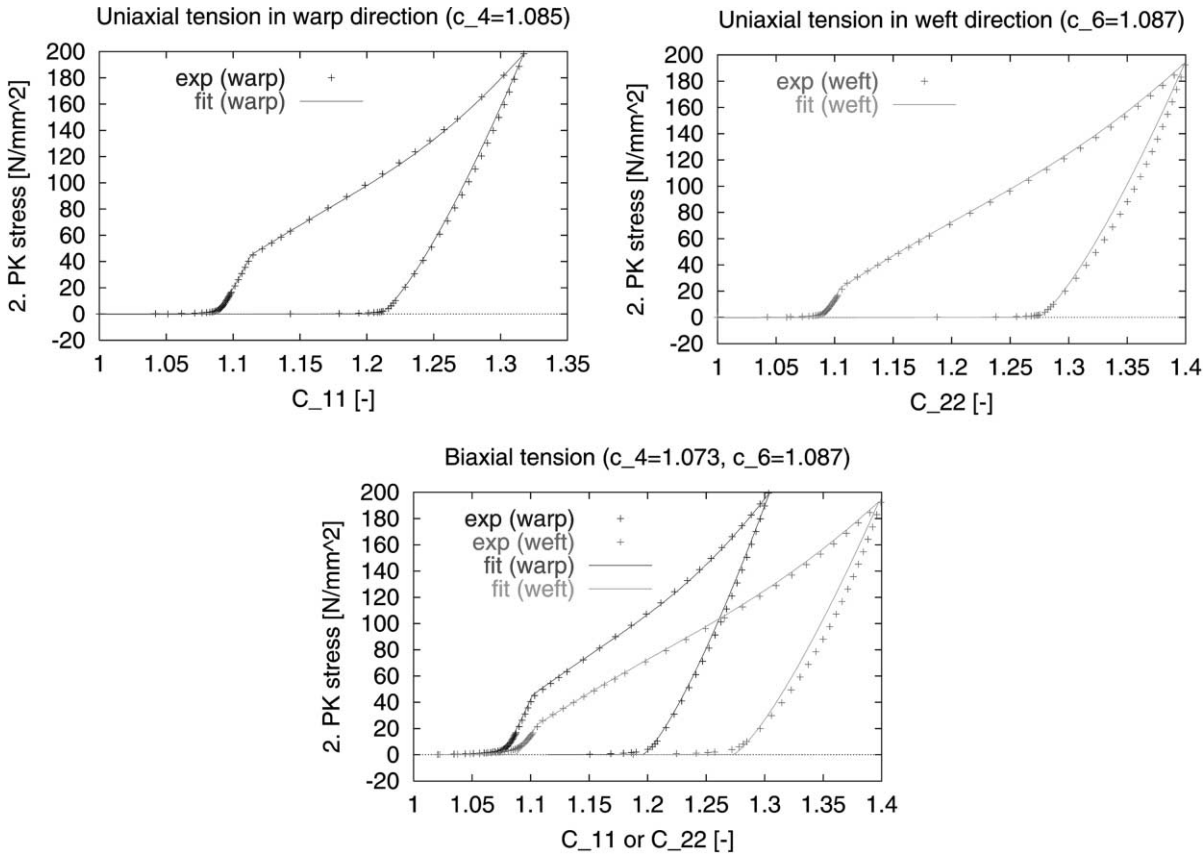

Fig. 7. Experimental results and fit for uniaxial and biaxial tension.

order to fulfill the dissipation inequality, it is important to clarify how the latter quantity is related to the stress tensor $\boldsymbol{\Sigma}$. After some steps, one obtains for $i = j$ $(i, j = 1, 2)$ the result

$$(\boldsymbol{\tau}_{\mathrm{iso}} + \boldsymbol{\tau}_{\mathrm{ani}\,i}) : \mathbf{m}_i = (\boldsymbol{\Sigma}_{\mathrm{iso}} + \boldsymbol{\Sigma}_{\mathrm{ani}\,j}) : \mathrm{sym}(\widetilde{\mathbf{M}}_j \cdot \mathbf{C}_{\mathrm{e}}) \frac{1}{I_{2j+2}}. \tag{25}$$

Note that Einstein's summation convention does not hold. However, it has to be emphasized that (25) does in general *not* hold for $i \neq j$. For a detailed derivation of the latter statement see Appendix C. Exceptions are the cases:

(a) The fibres remain orthogonal to each other ($\widetilde{\mathbf{N}}_1 \cdot \widetilde{\mathbf{N}}_2 = \mathbf{n}_1 \cdot \mathbf{n}_2 = 0$).
(b) The elastic part of the deformation is small ($\mathbf{b}_{\mathrm{e}} \approx \mathbf{1}$).

Looking at Fig. 1 it is recognized that assumption (b) is justified. Plastification begins at about 1% strain. In the computer model (see Fig. 5) the plastification in the fibres does not start before ≈5.5% strain which is due to the fact that the fibres are not stretched straight from the beginning. However, this difference with respect to the 1D consideration is due to the geometry of the computer model and should therefore not be included in the material modelling at this stage of the derivation. Thus, the choice $(i = 1, 2)$

$$\Phi_i = \left| \boldsymbol{\Sigma} : \mathrm{sym}(\widetilde{\mathbf{M}}_i \cdot \mathbf{C}_\mathrm{e}) \frac{1}{I_{2i+2}} \right| - \left(\sigma_{Yi} + H_{\mathrm{lin}\,i} \xi_i + H_{\mathrm{nl}\,i} \xi_i^{\chi_i} \right) \tag{26}$$

can be considered to be reasonable from the physical point of view. The coefficients q_i of $\mathbf{q} = q_i \mathbf{e}_i$ ($\mathbf{e}_i$ cartesian basis) are here given with $q_i = H_{\mathrm{lin}\,i} \xi_i + H_{\mathrm{nl}\,i} \xi_i^{\chi_i}$ $(i = 1, 2)$. The evolution equations are chosen as

$$\mathbf{d}_\mathrm{p} = \sum_{i=1}^{2} \dot{\gamma}_i \frac{\partial \Phi_i}{\partial \boldsymbol{\Sigma}} = \sum_{i=1}^{2} \dot{\gamma}_i \, \mathrm{sign} \left(\boldsymbol{\Sigma} : \mathrm{sym}(\widetilde{\mathbf{M}}_i \cdot \mathbf{C}_\mathrm{e}) \frac{1}{I_{2i+2}} \right) \mathrm{sym}(\widetilde{\mathbf{M}}_i \cdot \mathbf{C}_\mathrm{e}) \frac{1}{I_{2i+2}}, \qquad \dot{\xi}_i = \dot{\gamma}_i, \tag{27}$$

where the vector $\boldsymbol{\varepsilon}$ introduced in (17) is specified with $\boldsymbol{\varepsilon}^\mathrm{T} = \{\xi_1, \xi_2\}$. Above that, the Kuhn–Tucker conditions $\dot{\gamma}_i \geqslant 0$, $\Phi_i \leqslant 0$, $\dot{\gamma}_i \Phi_i = 0$ $(i = 1, 2)$ have to be fulfilled. Exploiting the residual dissipation inequality (17) yields

$$\sum_{i=1}^{2} \dot{\gamma}_i \left[\mathrm{sign} \left(\boldsymbol{\Sigma} : \mathrm{sym}(\widetilde{\mathbf{M}}_i \cdot \mathbf{C}_\mathrm{e}) \frac{1}{I_{2i+2}} \right) \right] \left[\boldsymbol{\Sigma} : \mathrm{sym}(\widetilde{\mathbf{M}}_i \cdot \mathbf{C}_\mathrm{e}) \frac{1}{I_{2i+2}} \right] + \dot{\gamma}_i \left(H_{\mathrm{lin}\,i} \xi_i + H_{\mathrm{nl}\,i} \xi_i^{\chi_i} \right) \geqslant 0. \tag{28}$$

Clearly, the inequality is always fulfilled, since the product of the sign-function with the scalar product as well as the plastic multiplier and the accumulated plastic strain are positive.

Although the expression $\boldsymbol{\tau} : \mathbf{m}_i$ cannot be completely transferred into an expression including $\boldsymbol{\Sigma}$, it would be certainly still preferable from the physical point of view to work with the yield criteria $(i = 1, 2)$

$$\Phi_i = |\boldsymbol{\tau} : \mathbf{m}_i| - \left(\sigma_{Yi} + H_{\mathrm{lin}\,i} \xi_i + H_{\mathrm{nl}\,i} \xi_i^{\chi_i} \right) \tag{29}$$

and the flow rule

$$-\frac{1}{2} \mathscr{L}_v \mathbf{b}_\mathrm{e} = \mathbf{F}_\mathrm{e} \cdot \mathbf{d}_\mathrm{p} \cdot \mathbf{F}_\mathrm{e}^\mathrm{T} = \sum_{i=1}^{2} \dot{\gamma}_i \, \mathrm{sign}(\boldsymbol{\tau} : \mathbf{m}_i) \, \mathrm{sym}(\mathbf{m}_i \cdot \mathbf{b}_\mathrm{e}) = \sum_{i=1}^{2} \dot{\gamma}_i \, \mathrm{sym} \left(\frac{\partial \Phi_i}{\partial \boldsymbol{\tau}} \cdot \mathbf{b}_\mathrm{e} \right). \tag{30}$$

It is obvious that in the case of Φ_i being an isotropic function of $\boldsymbol{\tau}$ and $\boldsymbol{\tau}$ being coaxial with $\mathbf{b}_\mathrm{e}$, we obtain the classical evolution equation for finite isotropic elastoplasticity written in terms of the Oldroyd derivative of $\mathbf{b}_\mathrm{e}$, the tensor $\mathscr{L}_v \mathbf{b}_\mathrm{e}$ (see Simo and Miehe, 1992).

It remains to show that also (30) fulfills the dissipation inequality. Inserting

$$\mathbf{d}_\mathrm{p} = -\frac{1}{2} \mathbf{F}_\mathrm{e}^{-1} \cdot \mathscr{L}_v \mathbf{b}_\mathrm{e} \cdot \mathbf{F}_\mathrm{e}^{-\mathrm{T}} = \sum_{i=1}^{2} \dot{\gamma}_i \, \mathrm{sign}(\boldsymbol{\tau} : \mathbf{m}_i) \, \mathrm{sym}(\widetilde{\mathbf{M}}_i \cdot \mathbf{C}_\mathrm{e}) \frac{1}{I_4} \tag{31}$$

into (17) leads to the requirement

$$\sum_{i=1}^{2} \dot{\gamma}_i \, \mathrm{sign}(\boldsymbol{\tau} : \mathbf{m}_i) \left[\boldsymbol{\Sigma} : \mathrm{sym}(\widetilde{\mathbf{M}}_i \cdot \mathbf{C}_\mathrm{e}) \frac{1}{I_{2i+2}} \right] + \dot{\gamma}_i \left(H_{\mathrm{lin}\,i} \xi_i + H_{\mathrm{nl}\,i} \xi_i^{\chi_i} \right) \geqslant 0. \tag{32}$$

Thus, if the statement

$$\mathrm{sign}(\boldsymbol{\tau} : \mathbf{m}_i) = \mathrm{sign} \left(\boldsymbol{\Sigma} : \mathrm{sym}(\widetilde{\mathbf{M}}_i \cdot \mathbf{C}_\mathrm{e}) \frac{1}{I_{2i+2}} \right) \tag{33}$$

holds, also (30) fulfills the dissipation inequality. The correctness of the statement (33) is proven in Appendix D.

If the fibre orientations remain orthogonal to each other during the deformation ($\mathbf{n}_1 \cdot \mathbf{n}_2 = 0$, $\widetilde{\mathbf{N}}_1 \cdot \widetilde{\mathbf{N}}_2 = 0$), both, $(27)_1$ and (30), reduce to

$$(\lambda_\mathrm{p})_i^{\cdot} = \dot{\gamma}_i \, \mathrm{sign} \tau_i (\lambda_\mathrm{p})_i. \tag{34}$$

This relation is equal to the evolution equation for the plastic stretch in the fibre model (see Table 1).

3.4. Parameter identification

The parameters of the material model presented in the Sections 3.1–3.3 are subsequently fitted to the computer experiments already discussed in Section 2 (see Fig. 7). The fit is at first restricted to uniaxial and biaxial tension. Obviously, the correlation between the "experimental" results and the results obtained with the continuum mechanical model is very good. At this point, however, one has to discuss the special geometry of the computer model. Due to the thickness of the computer test piece ($t = 0.3$ mm $= kL/n$ with $n = 10$ and $k = 0.3$, n number of fibres in each direction) the loading of the fibres does not begin before the test piece is deformed in such a way that the fibres are stretched straight. Since the original length of the fibres is computed with $L^{\mathrm{fib}} = L\sqrt{1+k^2}$, this deformation is described by the stretch $\lambda^{\star} = \sqrt{1+k^2}$ in each direction. But it has to be taken into consideration further that due to plastification, the length of the fibres as well as the dimensions of the computer model are increased in each load cycle. The multiplicative decomposition of the stretch in the fibre therefore reads

$$\lambda^{\mathrm{fib}} = \underbrace{\frac{L_{\mathrm{new}}}{L^{\mathrm{fib}} + \Delta L_{\mathrm{p}}}}_{\lambda_{\mathrm{e}}^{\mathrm{fib}}} \underbrace{\frac{L^{\mathrm{fib}} + \Delta L_{\mathrm{p}}}{L^{\mathrm{fib}}}}_{\lambda_{\mathrm{p}}^{\mathrm{fib}}}, \tag{35}$$

where ΔL_{p} is the lengthening of the whole model (including the fibres) due to plastification and L_{new} the current length of the whole model. The stretch of the computer model in one direction is described with (index i omitted)

$$\lambda = \underbrace{\frac{L_{\mathrm{new}}}{L + \Delta L_{\mathrm{p}}}}_{\lambda_{\mathrm{e}}} \underbrace{\frac{L + \Delta L_{\mathrm{p}}}{L}}_{\lambda_{\mathrm{p}}}. \tag{36}$$

$\lambda_{\mathrm{e}}^{\mathrm{fib}} = 1$ indicates the onset of the fibre loading. The associated elastic stretch $\lambda_{\mathrm{e}}^{\star}$ of the computer model is computed with

$$L_{\mathrm{new}} = L^{\mathrm{fib}} + \Delta L_{\mathrm{p}} \Rightarrow \lambda_{\mathrm{e}}^{\star} = \frac{L\sqrt{1+k^2} + \Delta L_{\mathrm{p}}}{L + \Delta L_{\mathrm{p}}}. \tag{37}$$

In the present computations, the plastic stretch hardly exceeds the value 1.1, i.e. the maximum of ΔL_{p} lies at about 0.1 L. $\lambda_{\mathrm{e}}^{\star}$ can therefore be approximated by the constant value

$$\lambda_{\mathrm{e}}^{\star} \approx \sqrt{1+k^2} \Rightarrow (C_{\mathrm{e}})_{11}^{\star} = (C_{\mathrm{e}})_{22} = (\lambda_{\mathrm{e}}^{\star})^2 \approx 1 + k^2. \tag{38}$$

Certainly, the value $\lambda_{\mathrm{e}}^{\star}$ is meaningless, if a rotation of the fibres takes place. For this reason, a relation between $\lambda_{\mathrm{e}}^{\mathrm{fib}}$ and the *invariants* I_m ($m = 4, \ldots, 7$) needs to be established:

- uniaxial and biaxial tension

$$[(C_{\mathrm{e}})_{ij}] = \begin{bmatrix} (C_{\mathrm{e}})_{11} & 0 & 0 \\ 0 & (C_{\mathrm{e}})_{22} & 0 \\ 0 & 0 & \approx (C_{\mathrm{e}})_{11}^{-1}(C_{\mathrm{e}})_{22}^{-1} \end{bmatrix}, \tag{39}$$

$$\Rightarrow I_4 = (C_{\mathrm{e}})_{11}, \qquad I_5 = (C_{\mathrm{e}})_{11}^2, \qquad I_6 = (C_{\mathrm{e}})_{22}, \qquad I_7 = (C_{\mathrm{e}})_{22}^2. \tag{40}$$

From that, we obtain

$$I_4^{\star} = I_6^{\star} = 1 + k^2, \qquad I_5^{\star} = I_7^{\star} = (1+k^2)^2. \tag{41}$$

- shearing

  The matrix of the deformation gradient **F** takes the form

$$[F_{ij}] = \begin{bmatrix} 1 & 0 & 0 \\ a & 1 & 0 \\ 0 & 0 & 1 \end{bmatrix}, \tag{42}$$

  where the parameter a represents the derivative of the displacement in vertical direction (u_2) with respect to X_1. The matrix of the right Cauchy–Green tensor is then computed with

$$[C_{ij}] = \begin{bmatrix} 1+a^2 & a & 0 \\ a & 1 & 0 \\ 0 & 0 & 1 \end{bmatrix}. \tag{43}$$

One obtains $I_4 = 1 + a^2$ and $I_6 = 1$. This result is physically reasonable, since the actual length of the fibre (if it is stretched straight) is computed with

$$L^{\text{fib}}_{\text{new}} = L\sqrt{1+a^2}. \tag{44}$$

If there is no plastic deformation, this yields for the stretch in the fibre the relation

$$\lambda^{\text{fib}} = \frac{L^{\text{fib}}_{\text{new}}}{L^{\text{fib}}} = \frac{\sqrt{1+a^2}}{\sqrt{1+k^2}}. \tag{45}$$

Thus, the loading of the fibre begins at $a = k = 0.3$ mm (30% shear strain). As it is the case for uniaxial or biaxial tension, the lengthening of the fibres due to plastic deformation would change this result slightly. The influence is again neglected, and we obtain independent of the fact, whether a pure stretching of the test piece or a shear deformation is considered, the result

$$I_4^{\star} = I_6^{\star} = 1 + k^2. \tag{46}$$

A problem arises due to the influence of the invariants I_5 and I_7. Considering again the special case of $\mathbf{C}_{\text{e}} = \mathbf{C}$, the invariant I_7 takes on the same value as I_4 which means that terms associated with I_7 would be switched on although the weft thread remains more or less undeformed. This difficulty can be circumvented by omitting the terms depending on I_5 and I_7 in W_{ani}. As fringe benefit, one obtains a major simplification of the model.

It turns out further that the coupling terms associated with the constants $K^{\text{kop}\,i}$ and $K^{\text{kop}\,12}$ are not needed to fit the computer results.

The strain energy term W_{ani} takes then the simple form ($c_{2i+2} \approx I^{\star}_{2i+2}$)

$$W_{\text{ani}} = K_1^{\text{ani}\,1}(I_4 - c_4)^{\beta_1} + K_1^{\text{ani}\,2}(I_6 - c_6)^{\gamma_1}, \tag{47}$$

where the parameters $K_1^{\text{ani}\,i}$ ($i = 1, 2$) are only unequal to zero, if $I_{2i+2} \geqslant c_{2i+2}$. The material parameters used to fit the experimental results in Fig. 7 are given below.

$$\begin{aligned} &K_1^{\text{ani}\,1} = 1000\,\text{N/mm}^2, \quad K_1^{\text{ani}\,2} = 1000\,\text{N/mm}^2, \quad \sigma_{Y1} = 50\,\text{N/mm}^2, \quad \sigma_{Y2} = 25\,\text{N/mm}^2, \\ &H_{\text{lin}\,1} = 2480\,\text{N/mm}^2, \quad H_{\text{lin}\,2} = 2150\,\text{N/mm}^2, \quad H_{\text{nl}\,1} = 65 \times 10^6\,\text{N/mm}^2, \quad H_{\text{nl}\,2} = 11 \times 10^6\,\text{N/mm}^2, \\ &\beta_1 = 2.3, \quad \gamma_1 = 2.3, \quad \chi_1 = 4.69, \quad \chi_2 = 4.69, \quad K_2^{\text{ani}\,i} = K_i^{\text{iso}} = K^{\text{kop}\,i} = K^{\text{kop}\,12} = 0, \qquad i = 1, 2. \end{aligned}$$

Note that the small strain stiffness is practically only determined by the Neo–Hooke part of the model, because the other parts of the stress are not active in this strain range. The Neo–Hooke parameters can therefore be chosen equal to the values in the computer model ($\mu = 1.4$ N/mm^2, $\Lambda = 300$ N/mm^2). It should

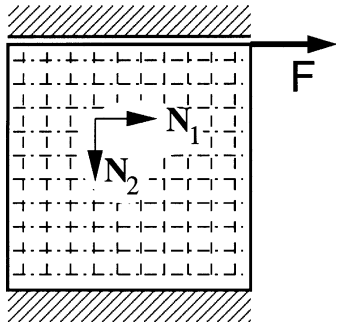

Fig. 8. Shear test.

be emphasized that the model is fit to the three experiments *simultaneously*. In this way, we obtain *one* set of parameters which shows a very good agreement for all three tests. An exception are the geometrical parameters c_4 and c_6 which take on different values in uniaxial and biaxial tension (see Fig. 7). The lower value of c_4 in biaxial tension is due to the effect of the weft fibres which are already stretched straight, when the loading in the warp fibres begins. It would also be possible to look at c_4 and c_6 as deformation-dependent functions, e.g. $c_4 = c_4(I_4, I_6)$, $c_6 = c_6(I_4, I_6)$. Such an idea should be investigated in further research.

At last, it is certainly important to test the model for the case that the fibres rotate. For this purpose, we look at the shearing of the computer test piece (see Fig. 8). The boundary conditions in the third coordinate direction are chosen such that a plane stress state is obtained.

In Fig. 9, the ''experimental'' results are compared with the results computed with the continuum mechanical model.

As pointed out in the above, only the warp thread is stretched such that only the terms including I_4 are effective. The elastic range and the onset of plastification are very well described. Note that the material parameters have not been fitted again. In the hardening range, the shear force computed with the continuum mechanical model increases slightly too quickly. Although the discrepancy is still tolerable, it might indicate that the use of only two scalar variables (ξ_1 and ξ_2) to describe the accumulated plastic strain could be too restrictive. This question should be also discussed in further work.

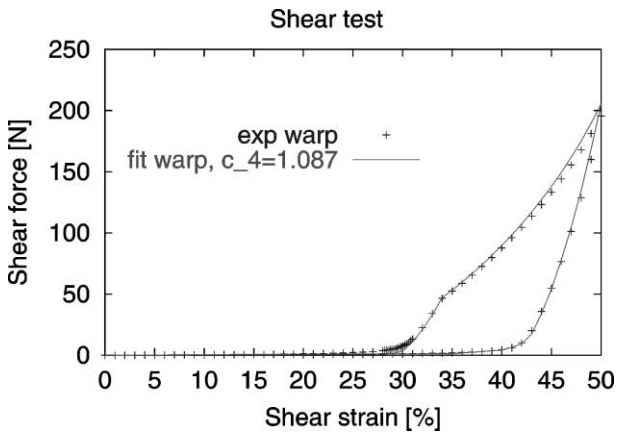

Fig. 9. Experimental results and fit for shear test.

4. Numerical aspects

4.1. Integration of the evolution equations

We introduce the short hand notation

$$a_i := -\dot{\gamma}_i \operatorname{sign}(\boldsymbol{\tau} : \mathbf{m}_i) \tag{48}$$

and reformulate (30) as

$$\mathscr{L}_v \mathbf{b}_e = \mathbf{F} \cdot \left(\frac{\mathrm{d}}{\mathrm{d}t} \mathbf{C}_p^{-1} \right) \cdot \mathbf{F}^T = \sum_{i=1}^{2} a_i (\mathbf{m}_i \cdot \mathbf{b}_e + \mathbf{b}_e \cdot \mathbf{m}_i). \tag{49}$$

Pulling back (49) to the reference configuration yields

$$\frac{\mathrm{d}}{\mathrm{d}t} \mathbf{C}_p^{-1} = \sum_{i=1}^{2} a_i \left(\mathbf{M}_i \cdot \mathbf{C} \cdot \mathbf{C}_p^{-1} + \mathbf{C}_p^{-1} \cdot \mathbf{C} \cdot \mathbf{M}_i \right) \frac{1}{\mathbf{C} : \mathbf{M}_i}. \tag{50}$$

The latter equation is now integrated by means of the backward Euler scheme leading to

$$\underbrace{\left(\frac{1}{2}\mathbf{1} - \sum_{i=1}^{2} \mathbf{M}_i \cdot \mathbf{C} \frac{a_i \Delta t}{\mathbf{C} : \mathbf{M}_i} \right)}_{\bar{\mathbf{A}}} \cdot \mathbf{C}_p^{-1} + \mathbf{C}_p^{-1} \cdot \underbrace{\left(\frac{1}{2}\mathbf{1} - \sum_{i=1}^{2} \mathbf{C} \cdot \mathbf{M}_i \frac{a_i \Delta t}{\mathbf{C} : \mathbf{M}_i} \right)}_{\bar{\mathbf{A}}^T} = \mathbf{C}_{pn}^{-1}. \tag{51}$$

Transferring this relation again to the current configuration gives

$$\mathbf{A} \cdot \mathbf{b}_e + \mathbf{b}_e \cdot \mathbf{A}^T = \mathbf{b}_e^{\mathrm{trial}}, \tag{52}$$

where the abbreviations

$$\mathbf{A} = \mathbf{F} \cdot \bar{\mathbf{A}} \cdot \mathbf{F}^{-1} = \frac{1}{2}\mathbf{1} - \sum_{i=1}^{2} a_i \Delta t \mathbf{m}_i \quad \text{and} \quad \mathbf{b}_e^{\mathrm{trial}} = \mathbf{F} \cdot \mathbf{C}_{pn}^{-1} \cdot \mathbf{F}^T \tag{53}$$

have been utilized. This integration rule is very advantageous from the computational point of view, since it represents a *linear* relation between $\mathbf{b}_e$ and $\mathbf{b}_e^{\mathrm{trial}}$ (note that $\mathbf{b}_e^{\mathrm{trial}}$ can be considered to be given at the Gauss point level). In index notation, (52) reads

$$A_{ik}(b_e)_{kj} + (b_e)_{ik}A_{jk} = (b_e^{\mathrm{trial}})_{ij} \Rightarrow \underbrace{(A_{ik}\delta_{jl} + A_{jk}\delta_{il})}_{\overline{D}_{ijkl}}(b_e)_{kl} = (b_e^{\mathrm{trial}})_{ij}. \tag{54}$$

Using the symmetry of $\mathbf{b}_e$, the matrix $\overline{D}_{ijkl}$ can be further symmetrized to read

$$D_{ijkl} = \tfrac{1}{2}(A_{ik}\delta_{jl} + A_{jk}\delta_{il} + A_{il}\delta_{jk} + A_{jl}\delta_{ik}). \tag{55}$$

In Voigt notation, the relation $\mathscr{D} : \mathbf{b}_e = \mathbf{b}_e^{\mathrm{trial}}$ is written as

$$\boldsymbol{b}_e = \boldsymbol{D}^{-1} \boldsymbol{b}_e^{\mathrm{trial}}, \tag{56}$$

with matrices (or vectors) denoted by slanted boldface letters. Since in the local integration procedure to be carried out at the Gauss point level, the deformation $\mathbf{F}$ and consequently also the structural tensors $\mathbf{m}_i$ are held constant, $\mathscr{D}$ contains the slip rates $\dot{\gamma}_i$ $(i = 1, 2)$ as only unknowns.

In summary, at the Gauss point level, we have to solve the following equations ($\Delta\gamma_i := \dot{\gamma}_i \Delta t$):

$$\begin{aligned} &\mathbf{r}(\mathbf{b}_e, \Delta\gamma_1, \Delta\gamma_2) = \boldsymbol{b}_e - \boldsymbol{D}^{-1}\boldsymbol{b}_e^{\text{trial}} = \mathbf{0}, \\ &s_i(\xi_i, \Delta\gamma_i) = \xi_i - \xi_{in} - \Delta\gamma_i = 0, \\ &\Phi_i(\hat{\boldsymbol{\tau}}(\boldsymbol{b}_e), \xi_i) = 0. \end{aligned} \tag{57}$$

Note that the Voigt notation of $\boldsymbol{\tau}$ is indicated by $\hat{\boldsymbol{\tau}}$. The use of $(57)_1$ and $(57)_2$ in $(57)_3$ leads to

$$\Phi_i(\Delta\gamma_1, \Delta\gamma_2) = \left| \boldsymbol{m}_i^{\mathrm{T}} \hat{\boldsymbol{\tau}}\left(\boldsymbol{D}(\Delta\gamma_1, \Delta\gamma_2)^{-1} \boldsymbol{b}_e^{\text{trial}} \right) \right| - \underbrace{\left(\sigma_{Yi} + H_{\text{lin}\,i}(\xi_{in} + \Delta\gamma_i) + H_{\text{nl}\,i}(\xi_{in} + \Delta\gamma_i)^{\chi_i} \right)}_{f_i(\Delta\gamma_i)} = 0. \tag{58}$$

Thus, the local 10×10 equation system reduces to the iterative solution of two non-linear scalar equations. The remaining unknowns are determined by directly evaluating the functional relations.

4.2. Local Newton iteration

In order to apply Newton's method to solve (58), the consistent linearization of (58) with respect to $\Delta\gamma_1$ and $\Delta\gamma_2$ is necessary. In the present case, it is, however, numerically inefficient to compute the tangent analytically, since it involves many multiplications of 6×6 matrices. Instead, we use the classical numerical tangent which represents a scalar or, in the most complicated case, a 2×2 matrix.

Additionally important is the fact that one has to deal here with a simple kind of multisurface plasticity, where a differentiation between the following four cases has to be carried out:

(1) $\Phi_1 < 0$, $\Phi_2 < 0$: no further plastification;
(2) $\Phi_1 = 0$, $\Phi_2 < 0$: further plastification in the warp fibre;
(3) $\Phi_1 < 0$, $\Phi_2 = 0$: further plastification in the weft fibre;
(4) $\Phi_1 = 0$, $\Phi_2 = 0$: further plastification in both fibres.

Depending on the sign of the start values Φ_i^{trial} $(i = 1, 2)$ at the beginning of the iteration, one proceeds into the Newton loops for the Cases (2)–(4). Case (1) means that no further plastification occurs. The loops for Cases (2) and (3) involve the iterative solution of either $\Phi_1 = 0$ (Case (2), active set: 1) or $\Phi_2 = 0$ (Case (3), active set: 2). In Case (4), both equations, $\Phi_1 = 0$ and $\Phi_2 = 0$, have to be solved simultaneously. The active set includes the systems 1 and 2. During the iteration, negative values of $\Delta\gamma_1$ or $\Delta\gamma_2$ might occur. In order to avoid this problem, the side condition $\Delta\gamma_i = \max(0, \Delta\gamma_i)$ is introduced. If no solution of (58) can be found, the active set has to be modified according to the value of $\Delta\gamma_1$ and $\Delta\gamma_2$ at the end of the failed iteration. See for more information about the active set strategy in the large strain domain the references Cuitino and Ortiz (1992) and Miehe (1996).

4.3. Solution of the weak form

The weak form of the balance of linear momentum reads

$$g(\mathbf{u}, \delta\mathbf{u}) = \int_{\mathscr{B}_0} \mathbf{P} : \delta\mathbf{F}\, \mathrm{d}V - g_a = 0, \tag{59}$$

where $\mathbf{P} = \mathbf{F} \cdot \mathbf{S}(\mathbf{C}, \mathbf{C}_p(\mathbf{C}))$ denotes the first Piola–Kirchhoff stress tensor, $\delta\mathbf{F} = \mathrm{Grad}\,\delta\mathbf{u}$ the variation of the deformation gradient and $\mathrm{d}V$ a volume element in the undeformed configuration $\mathscr{B}_0$. Applying the numerical integration procedure introduced in Section 4.1, the second Piola–Kirchhoff stress tensor $\mathbf{S}$ is seen at the global finite element level as a function of the right Cauchy–Green tensor $\mathbf{C}$ only. Further, g_a

represents a short hand notation for the virtual work of the external loading. The consistent linearization of (59) yields

$$g(\mathbf{u},\delta\mathbf{u}) \approx g(\bar{\mathbf{u}},\delta\mathbf{u}) + \Delta g(\bar{\mathbf{u}},\delta\mathbf{u}) = 0 \tag{60}$$

with

$$\Delta g(\mathbf{u},\delta\mathbf{u}) = \int_{\mathscr{B}_0} \left(\underbrace{\frac{\partial \mathbf{P}}{\partial \mathbf{F}}}_{\mathscr{A}} : \Delta\mathbf{F} \right) : \delta\mathbf{F}\, \mathrm{d}V + \Delta g_a. \tag{61}$$

In the finite element computations, the matrix form $\mathbf{A}$ of the tangent tensor $\mathscr{A}$ is replaced by the numerical approximation

$$A_{ij} = \frac{P_i(F_1,\ldots,F_j+\varepsilon,\ldots,F_9) - P_i(F_1,\ldots,F_j,\ldots,F_9)}{\varepsilon}. \tag{62}$$

Note that for this purpose, $\mathbf{P}$ and $\mathbf{F}$ have been formulated in vector form. The parameter ε is chosen equal to 10^{-8}.

5. Examples

In this section, two examples are discussed for the purposes (1) to study the behaviour of the composite material in more general deformation and stress states and (2) to validate the finite element implementation. Due to the rather high numerical effort at the element level, typical for sophisticated material models, it is suitable to work with one Gauss point element formulations. For various kinds of hourglass stabilizations refer to Reese et al. (1999, 2000).

5.1. Inflation of a rectangular membrane

Pneumatic structures obtain their stability by inflation, i.e. they are exposed to a deformation-dependent pressure loading p (see e.g. Schweizerhof and Ramm, 1984). Frequently, pieces with different fibre orientations are sewed together.

In the left half of the system (Fig. 10), the fibers are lying in horizontal and vertical directions (0°/90°, solid line: warp thread, dashed line: weft thread). In the right half, the orientation angles −45°/+45° are chosen. At the boundaries defined by $X_1 = 0$ mm, $X_1 = 10$ mm, $X_2 = 0$ mm and $X_2 = 16$ mm, all degrees-of-freedom are fixed.

In Fig. 11, the evolution of the Kirchhoff stress in the direction of X_1 is shown. It is clearly visible that a stress concentration arises in the neighbourhood of the seam. In general, τ_{11} reaches much higher values than τ_{22} (Fig. 12).

Looking in addition at the deformed system (Fig. 13), it is evident that the left side of the membrane (fibre orientations 0°/90°) shows noticeably stiffer behaviour than the right hand side (fibre orientations 45°/−45°).

It is further interesting to observe the evolution of the plastic deformation. The plots in Fig. 14 (Fig. 15) show the regions, where $\Phi_1 = 0$, $\Phi_2 < 0$ ($\Phi_2 = 0$, $\Phi_1 < 0$) hold. The plastification starts in the area of the stress concentration which is a physically reasonable result.

At $p = 1.21$ N/mm^2, there is a very small region (not shown in the plots), where both slip systems are active ($\Phi_1 = \Phi_2 = 0$). This region increases, however, quickly, until in almost the entire system, plastification occurs in both directions (Fig. 16).

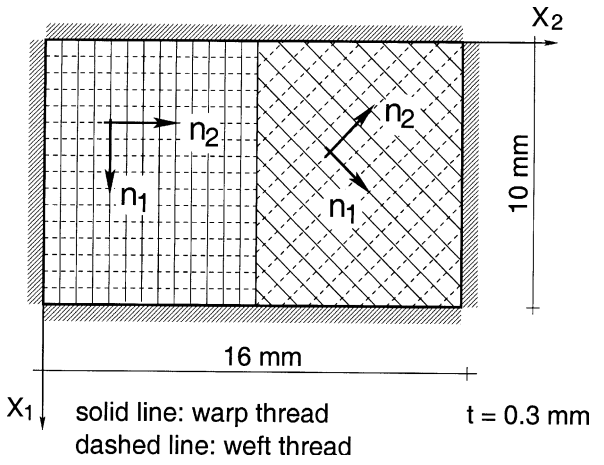

Fig. 10. Rectangular membrane, geometry and boundary conditions.

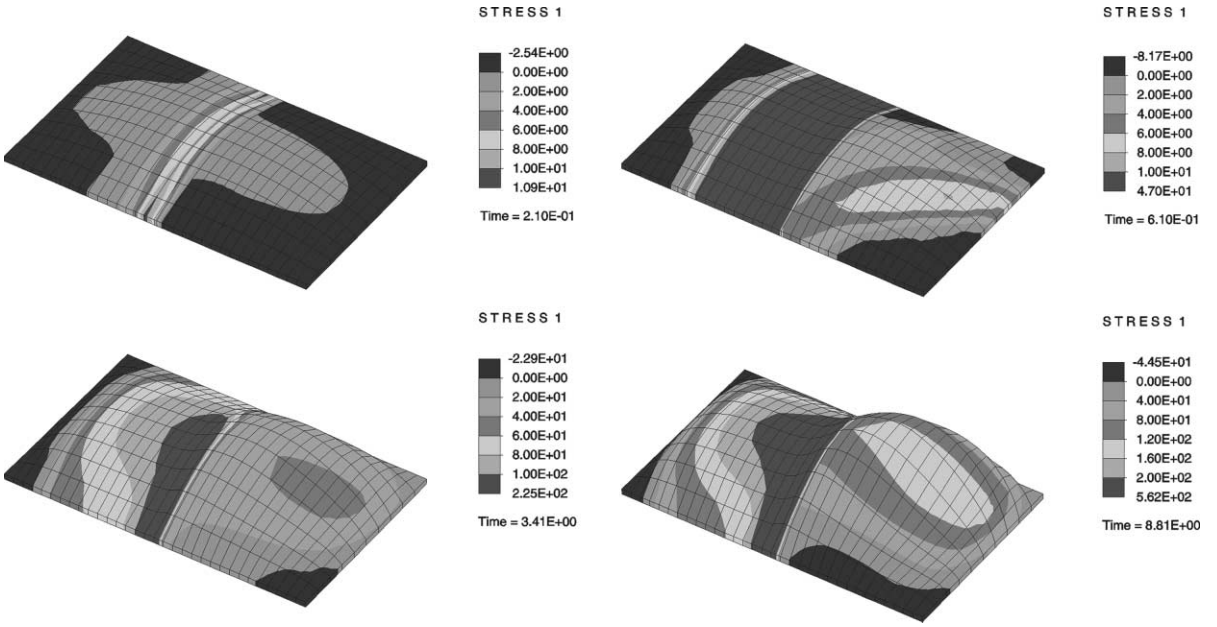

Fig. 11. Kirchhoff stress τ_{11} for different load states ($p = 0.21$, 0.61, 3.41, 8.81 N/mm^2).

5.2. Pneumatic column

In the second example, the deformation behaviour of a classical pneumatic construction element is investigated in detail. The geometry of the discretized system is shown in Fig. 17.

Only one half of the column is discretized. The pressure loading p acting on the inner side of the column is visible in the middle part of Fig. 17. In addition, a vertical force F pointing in the negative z-direction is

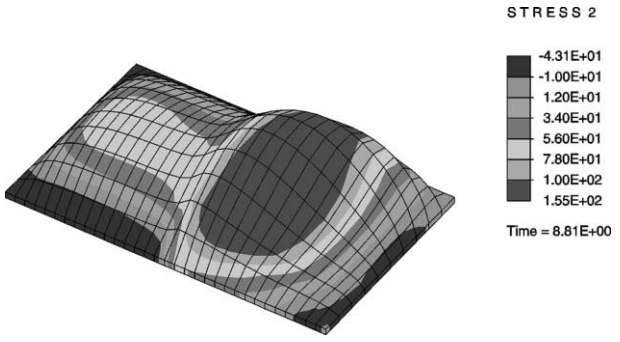

Fig. 12. Kirchhoff stress τ_{22} for $p = 8.81$ N/mm^2.

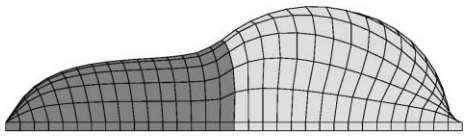

Fig. 13. Deformed system for $p = 8.81$ N/mm^2, different perspective.

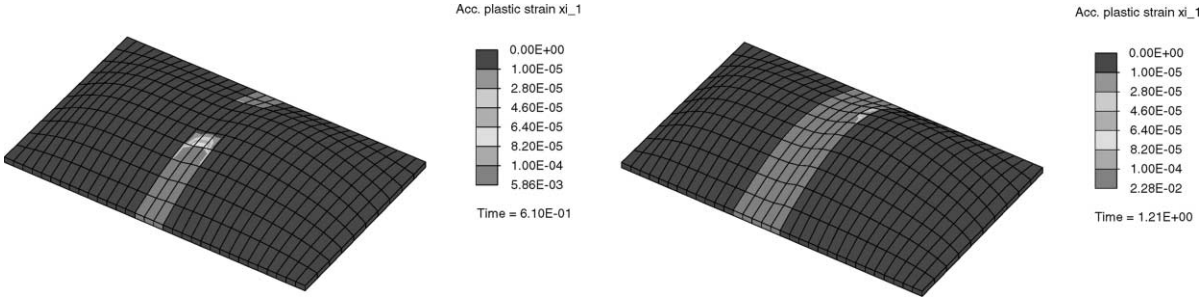

Fig. 14. Accumulated plastic strain ξ_1 for different load states ($\Phi_1 = 0$, $\Phi_2 < 0$).

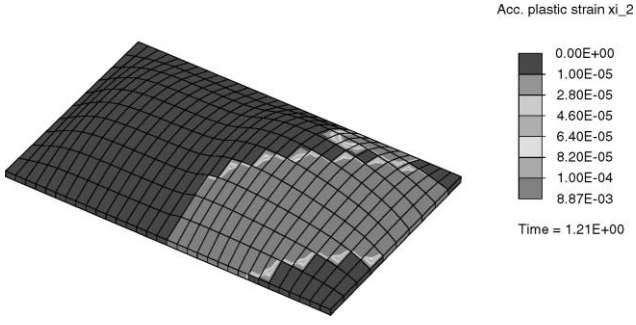

Fig. 15. Accumulated plastic strain ξ_2 for $p = 1.21$ N/mm^2 ($\Phi_2 = 0$, $\Phi_1 < 0$).

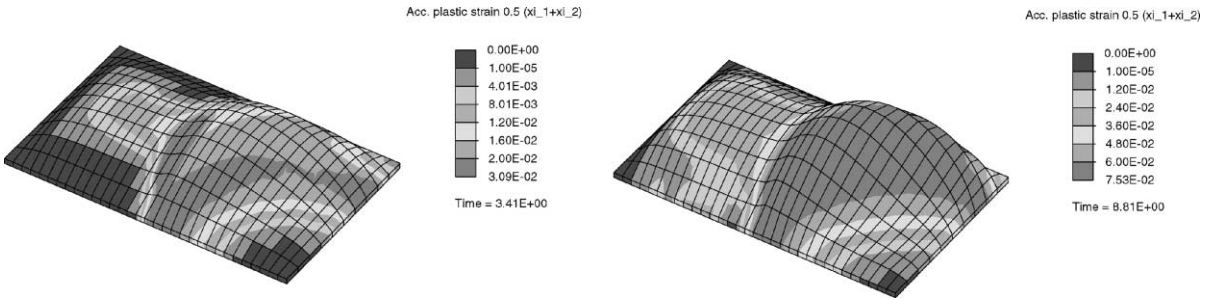

Fig. 16. Average accumulated plastic strain $\frac{1}{2}(\xi_1 + \xi_2)$ for different load states ($\Phi_1 = 0$, $\Phi_2 = 0$).

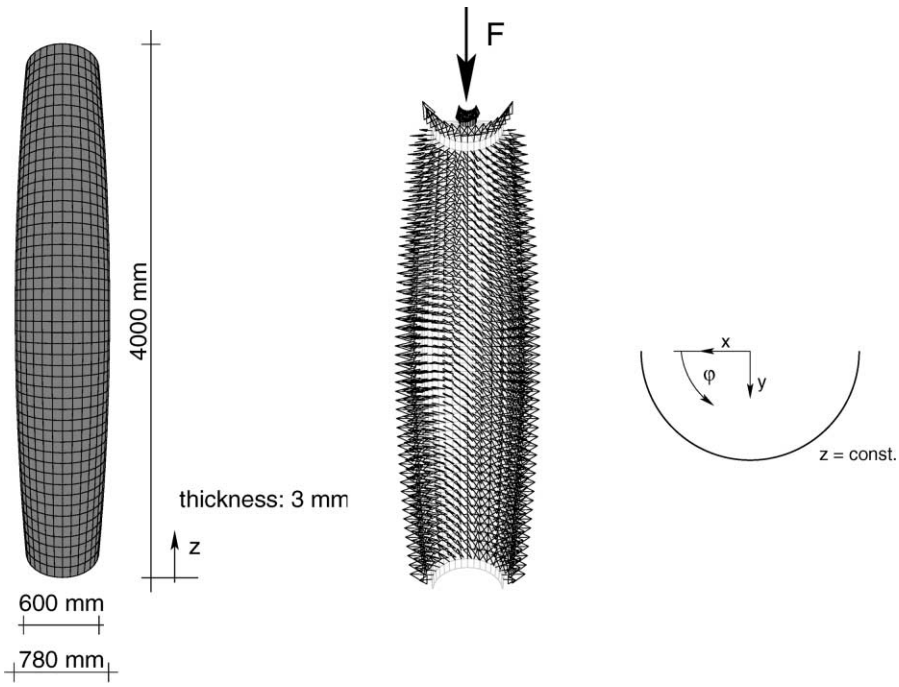

Fig. 17. Pneumatic column, (a) geometry, (b) pressure loading, (c) cross-section.

applied at the top. At the bottom of the structure ($z = 0$), all three degrees-of-freedom (the displacements in the three coordinate directions) are fixed. The system is covered with a top made of usual rubber material ($\mu = 1.4$ N/mm^2, $\Lambda = 1000$ N/mm^2). The pressure loading is also applied at the inside of this cover contributing to the vertical loading of the system. The third degrees-of-freedom (displacements in z-direction, i.e. w) at the top of the structure ($z = 4000$ and 4003 mm) are linked together, the cover therefore maintains always its horizontal orientation. It is further assumed that the nodes lying in the plane $y = 0$ (see right part of Fig. 17) do not move in y-direction. The displacement in x-direction is hindered at $x = 0$, $z = 4000$ mm and $x = 0$, $z = 4003$ mm.

In the first computation, we study the deformation behaviour of the column for different fibre orientations. The loading is applied in two-phases:

(1) inflation of the column: increase of the internal pressure p up to a certain value $\bar{p}$,
(2) vertical loading of the column: the pressure is held constant ($p = \bar{p}$), increase of the vertical force F.

In Fig. 18, the deformed configurations of the column, including the contours for the displacement w, are shown for different fibre orientations (load state: end of phase (1), here: $\bar{p} = 0.6011$ N/mm^2). The maximum and minimum values in mm are listed in Table 2 (columns a). Obviously, the angle of the contour lines is almost identical with the orientation of the warp thread.

The contours of the Kirchhoff stress in z-direction τ_{33} are plotted in Fig. 19, for the max/min values refer to Table 2 (columns b). For the orientations 70°/−20°, 65°/−25° and 60°/−30°, the maximum values of τ_{33} are found in the vicinity of the plane $y = 0$. In contrast to the computations based on the angles 90°/0° and 45°/−45°, compressive stresses occur which cause wrinkling effects at the top and at the bottom of the structure.

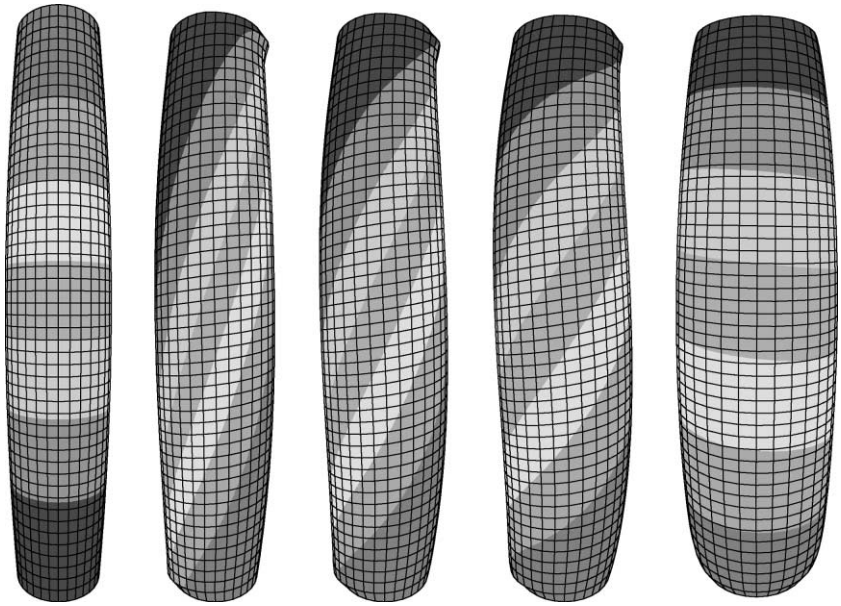

Fig. 18. Contour plots of w, fibre orientations: (a) 90°/0°, (b) 70°/−20°, (c) 65°/−25°, (d) 60°/−30°, (e) 45°/−45°.

Table 2
Maximum/minimum values of w (a) and τ_{33} (b)

Orientation	(a)		(b)	
	max w	min w	max τ_{33}	min τ_{33}
90°/0°	44.8	−1.23	56.2	0
70°/−20°	9.57	−172	66.5	−3.38
65°/−25°	0.90	−305	62.5	−2.66
60°/−30°	0	−478	55.5	−2.27
45°/−45°	0	−861	38.0	0

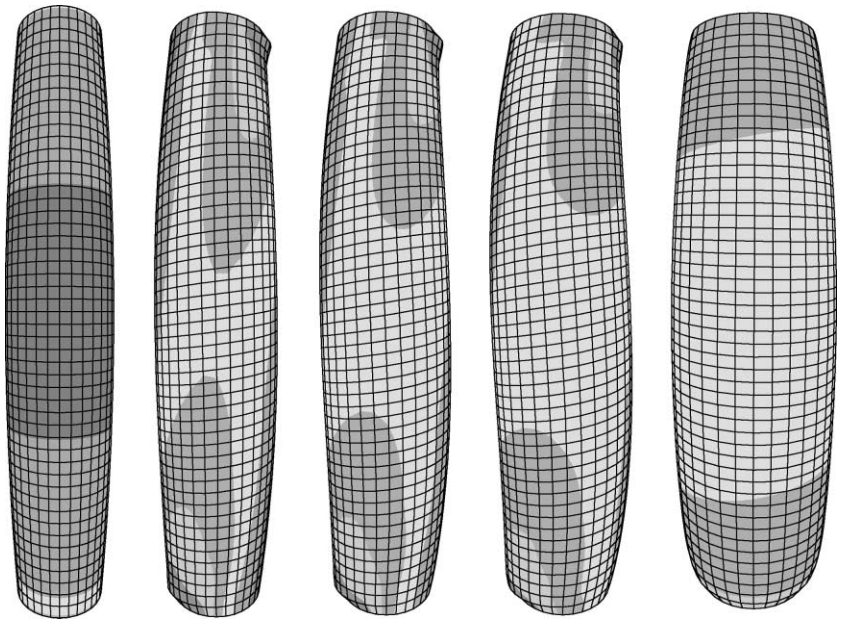

Fig. 19. Contour plots of the Kirchhoff stress τ_{33}, fibre orientations: (a) 90°/0°, (b) 70°/−20°, (c) 65°/−25°, (d) 60°/−30°, (e) 45°/−45°.

It is further interesting to compare the process of plastification for different fibre orientations. In Fig. 20, one sees the regions, where $\Phi_1 < 0$, $\Phi_2 = 0$ hold. The domain, where both slip systems are active ($\Phi_1 = \Phi_2 = 0$), is plotted in Fig. 21. In the dark region, the accumulated strain, (ξ_2 or $\frac{1}{2}(\xi_1 + \xi_2)$, respectively), is smaller than 10^{-5}. The maximum values are given in Table 3. Obviously, the smaller the angle of the warp thread, the larger becomes the region with $\Phi_1 = \Phi_2 = 0$.

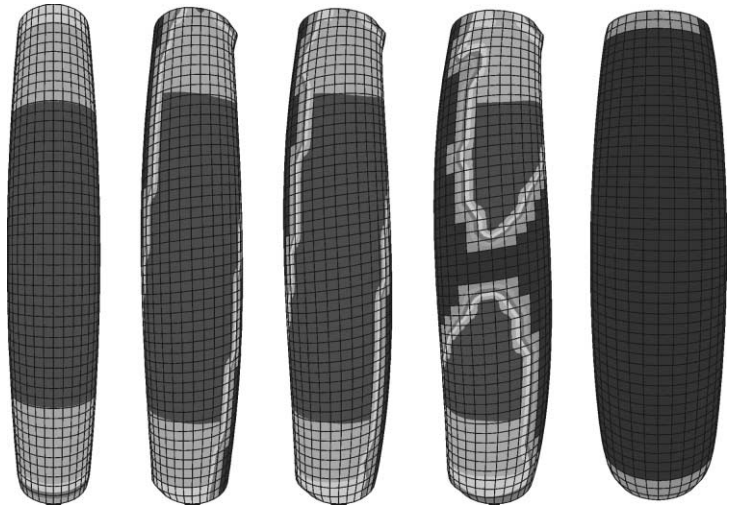

Fig. 20. Accumulated plastic strain ξ_2 ($\Phi_1 < 0$, $\Phi_2 = 0$), fibre orientations: (a) 90°/0°, (b) 70°/−20°, (c) 65°/−25°, (d) 60°/−30°, (e) 45°/−45°.

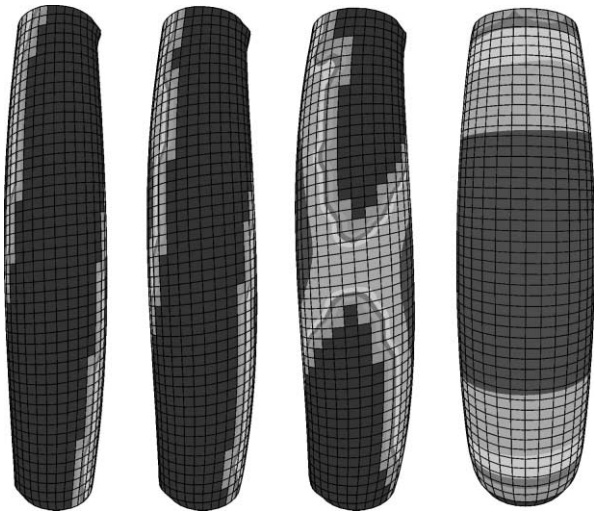

Fig. 21. Accumulated plastic strain $\frac{1}{2}(\xi_1 + \xi_2)$ ($\Phi_1 = 0$, $\Phi_2 = 0$), fibre orientations: (b) 70°/−20°, (c) 65°/−25°, (d) 60°/−30°, (e) 45°/−45°.

Finally, it remains to investigate how the system behaves in load phase (2). The force–displacement curves for different fibre orientations are plotted in Fig. 22. The letter w refers to the displacement of the top of the structure in the negative z-direction. It is counted from the end of phase (1) ($w = 0$). For the angles 90°/0°, an almost linear relationship between F and w is obtained (solid curve). The kink indicates the load state, when compressive stresses occur for the first time. At a slightly increased load, the system loses its stability. Interestingly, other fibre orientations as 70°/−20° and 65°/−25° lead to stiffer behaviour of the membrane for loads in the range of 0–2.5 kN. Beyond this limit, the influence of the compressive stresses in the system becomes too severe causing instabilities due to wrinkling. If one chooses the fibre orientations 60°/−30° and 45°/−45°, the system is rather soft in load phase (1). At the beginning of load phase (2), negative values of w occur for small values of F. Thus, the top of the structure moves upwards, although the load F is directed in the opposite direction. This can be explained by the fact that the stress components τ_{ii} ($i = 1, 2, 3$) decrease with increasing F, causing the system to relax.

One important point, however, should be mentioned at last. The pneumatic column can be seen as a closed system, where the equation of state for an ideal gas $pV = nk\Theta$ (V enclosed volume, n number of molecules, k Boltzmann's constant, Θ absolute temperature) has to be fulfilled. For isothermal processes, it boils down to the statement $pV =$ constant. Increasing the load F results due to the unloading of the fibres to a decrease of the volume. According to the gas equation, the pressure must increase leading eventually to a further loading of the fibres. On the other hand, the volume might increase accompanied by a decrease of

Table 3
Maximum values of ξ_2 (a) and $\frac{1}{2}(\xi_1 + \xi_2)$ (b)

Orientation	(a) $\max \xi_2$	(b) $\max \frac{1}{2}(\xi_1 + \xi_2)$
90°/0°	2.84×10^{-2}	Φ_1 not active
70°/−20°	2.92×10^{-2}	1.65×10^{-2}
65°/−25°	2.93×10^{-2}	1.68×10^{-2}
60°/−30°	1.69×10^{-2}	1.69×10^{-2}
45°/−45°	1.15×10^{-2}	1.71×10^{-2}

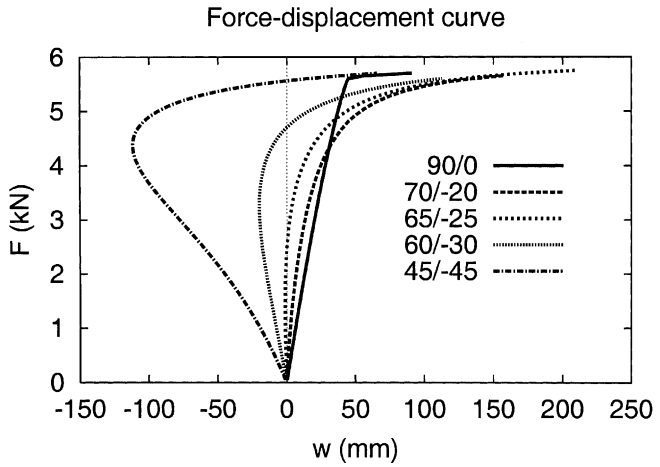

Fig. 22. Force–displacement curves for load phase (2), different fibre orientations.

the pressure. From the engineering point of view, however, it can be assumed that the first situation is more realistic. Then, negative stiffnesses of the column as shown in Fig. 22 could not occur. The gas equation can be included int the finite element implementation by treating the pressure as additional degree-of-freedom (see e.g. the recent work of Rumpel and Schweizerhof, in press). The application of such an algorithm in the context of pneumatic membranes is currently under investigation.

6. Conclusions

The main goal of this paper has been to model the anisotropically elastoplastic material behaviour of fibre-reinforced membranes. Due to the lack of enough experimental data, a computer model has been set up. Simulating various biaxial and uniaxial experiments with such a "virtual" test piece, we are able to generate sufficient test data. As an additional benefit, one gains a deeper understanding of what happens inside the material.

It is crucial to consider plastic deformations in order to obtain a realistic description of the material behaviour. Interestingly, one can show that based on the assumption that the structural vectors transform like material line elements, the plastic deformation is represented by means of a symmetric tensor-valued internal variable. Thus, the plastic spin remains undetermined. This is a surprising result in the context of anisotropic material behaviour. The integration of the material equations is efficiently achieved via a backward Euler scheme applied in the framework of a return-mapping algorithm. The finite element implementation can therefore be carried out in a straightforward manner. The numerical investigation of an inflated pneumatic column shows that the fibre orientation has an important influence on the resulting force–displacement curves.

Acknowledgements

The author wishes to thank Bob Svendsen (University of Dortmund, Germany) and Tilmann Raible (University of Hannover, Germany) for useful discussions on important aspects of this work.

Appendix A

In this appendix, the computation of the Kirchhoff stress tensor $\boldsymbol{\tau}$ is shown in detail.

- Derivative of W with respect to $\mathbf{C}_e$

$$\frac{\partial W}{\partial \mathbf{C}_e} = \frac{\partial W}{\partial I_1}\frac{\partial I_1}{\partial \mathbf{C}_e} + \frac{\partial W}{\partial I_2}\frac{\partial I_2}{\partial \mathbf{C}_e} + \frac{\partial W}{\partial I_3}\frac{\partial I_3}{\partial \mathbf{C}_e} + \frac{\partial W}{\partial I_4}\frac{\partial I_4}{\partial \mathbf{C}_e} + \frac{\partial W}{\partial I_5}\frac{\partial I_5}{\partial \mathbf{C}_e} + \frac{\partial W}{\partial I_6}\frac{\partial I_6}{\partial \mathbf{C}_e} + \frac{\partial W}{\partial I_7}\frac{\partial I_7}{\partial \mathbf{C}_e}, \tag{A.1}$$

$$\frac{\partial I_1}{\partial \mathbf{C}_e} = \mathbf{1}, \qquad \frac{\partial I_2}{\partial \mathbf{C}_e} = I_1\mathbf{1} - \mathbf{C}_e, \qquad \frac{\partial I_3}{\partial \mathbf{C}_e} = I_3\mathbf{C}_e^{-1}, \tag{A.2}$$

$$\frac{\partial I_{2i+2}}{\partial \mathbf{C}_e} = \widetilde{\mathbf{M}}_i, \qquad \frac{\partial I_{2i+3}}{\partial \mathbf{C}_e} = \mathbf{C}_e \cdot \widetilde{\mathbf{M}}_i + \widetilde{\mathbf{M}}_i \cdot \mathbf{C}_e. \tag{A.3}$$

- Definition of $\overline{\mathbf{m}}_i$

$$\overline{\mathbf{m}}_i = \mathbf{F}_e \cdot \widetilde{\mathbf{M}}_i \cdot \mathbf{F}_e^T = \frac{\mathbf{F}\cdot\mathbf{M}_i\cdot\mathbf{F}^T}{\mathbf{C}:\mathbf{M}_i}\frac{\mathbf{C}:\mathbf{M}_i}{\mathbf{C}_p:\mathbf{M}_i} = \mathbf{m}_i I_{2i+2}. \tag{A.4}$$

- Kirchhoff stress tensor

$$\begin{aligned}\boldsymbol{\tau} &= 2\mathbf{F}_e\cdot\frac{\partial W}{\partial \mathbf{C}_e}\cdot\mathbf{F}_e^T \\ &= 2\frac{\partial W}{\partial I_1}\mathbf{b}_e + 2\frac{\partial W}{\partial I_2}(I_1\mathbf{b}_e - \mathbf{b}_e^2) + 2\frac{\partial W}{\partial I_3}I_3\mathbf{1} && \text{(A.5)}\\ &\quad + 2\frac{\partial W}{\partial I_4}\overline{\mathbf{m}}_1 + 2\frac{\partial W}{\partial I_5}(\mathbf{b}_e\cdot\overline{\mathbf{m}}_1 + \overline{\mathbf{m}}_1\cdot\mathbf{b}_e) && \text{(A.6)}\\ &\quad + 2\frac{\partial W}{\partial I_6}\overline{\mathbf{m}}_2 + 2\frac{\partial W}{\partial I_7}(\mathbf{b}_e\cdot\overline{\mathbf{m}}_2 + \overline{\mathbf{m}}_2\cdot\mathbf{b}_e). && \text{(A.7)}\end{aligned}$$

Appendix B

In this appendix, the computation of the stress tensor $\boldsymbol{\Sigma}$ is discussed. In the course of this, the symmetry of this tensor comes out as another important result.

- Derivation of the derivative $\partial W/\partial \mathbf{F}_p$

$$DW(\mathbf{C}_e, \widetilde{\mathbf{M}}_1, \widetilde{\mathbf{M}}_2) : \dot{\mathbf{F}}_p = -\frac{\partial W}{\partial \mathbf{C}_e} : \left(\mathbf{C}_e\cdot\mathbf{l}_p + \mathbf{l}_p^T\cdot\mathbf{C}_e\right) + \frac{\partial W}{\partial \widetilde{\mathbf{M}}_1} : (\widetilde{\mathbf{M}}_1)^{\cdot} + \frac{\partial W}{\partial \widetilde{\mathbf{M}}_2} : (\widetilde{\mathbf{M}}_2)^{\cdot}, \tag{B.1}$$

$$(\widetilde{\mathbf{M}}_i)^{\cdot} = \left(\dot{\mathbf{F}}_p\cdot\mathbf{M}_i\cdot\mathbf{F}_p^T + \mathbf{F}_p\cdot\mathbf{M}_i\cdot\dot{\mathbf{F}}_p^T\right)\frac{1}{\mathbf{C}_p:\mathbf{M}_i} - \frac{\dot{\mathbf{C}}_p:\mathbf{M}_i}{\mathbf{C}_p:\mathbf{M}_i}\widetilde{\mathbf{M}}_i. \tag{B.2}$$

- Intermediate result

$$\begin{aligned}\frac{\dot{\mathbf{C}}_p:\mathbf{M}_i}{\mathbf{C}_p:\mathbf{M}_i} &= \left(\dot{\mathbf{F}}_p^T\cdot\mathbf{F}_p + \mathbf{F}_p^T\cdot\dot{\mathbf{F}}_p\right):\mathbf{M}_i\frac{1}{\mathbf{C}_p:\mathbf{M}_i} \\ &= \left(\mathbf{F}_p^T\cdot\mathbf{F}_p^{-T}\cdot\dot{\mathbf{F}}_p^T\cdot\mathbf{F}_p + \mathbf{F}_p^T\cdot\dot{\mathbf{F}}_p\cdot\mathbf{F}_p^{-1}\cdot\mathbf{F}_p\right):\mathbf{M}_i\frac{1}{\mathbf{C}_p:\mathbf{M}_i} = \left(\mathbf{l}_p^T + \mathbf{l}_p\right):\widetilde{\mathbf{M}}_i = 2\mathbf{d}_p:\widetilde{\mathbf{M}}_i. \end{aligned}\tag{B.3}$$

- Time derivative of $\widetilde{\mathbf{M}}_i$

$$(\widetilde{\mathbf{M}}_i)^{\cdot} = \mathbf{l}_\mathrm{p} \cdot \widetilde{\mathbf{M}}_i + \widetilde{\mathbf{M}}_i \cdot \mathbf{l}_\mathrm{p}^\mathrm{T} - 2(\mathbf{d}_\mathrm{p} : \widetilde{\mathbf{M}}_i)\widetilde{\mathbf{M}}_i. \tag{B.4}$$

- Final result for

$$\begin{aligned} &DW(\mathbf{C}_\mathrm{e}, \widetilde{\mathbf{M}}_1, \widetilde{\mathbf{M}}_2) : \dot{\mathbf{F}}_\mathrm{p} \\ &\quad = 2\left(-\mathbf{C}_\mathrm{e} \cdot \frac{\partial W}{\partial \mathbf{C}_\mathrm{e}} + \frac{\partial W}{\partial \widetilde{\mathbf{M}}_1} \cdot \widetilde{\mathbf{M}}_1 + \frac{\partial W}{\partial \widetilde{\mathbf{M}}_2} \cdot \widetilde{\mathbf{M}}_2 - \frac{\partial W}{\partial \widetilde{\mathbf{M}}_1} : (\widetilde{\mathbf{M}}_1 \otimes \widetilde{\mathbf{M}}_1) - \frac{\partial W}{\partial \widetilde{\mathbf{M}}_2} : (\widetilde{\mathbf{M}}_2 \otimes \widetilde{\mathbf{M}}_2) \right) : \mathbf{l}_\mathrm{p}. \end{aligned} \tag{B.5}$$

- Stress tensor $\boldsymbol{\Sigma}$

$$\boldsymbol{\Sigma} = 2\mathbf{C}_\mathrm{e} \cdot \frac{\partial W}{\partial \mathbf{C}_\mathrm{e}} - 2\frac{\partial W}{\partial \widetilde{\mathbf{M}}_1} \cdot \widetilde{\mathbf{M}}_1 - 2\frac{\partial W}{\partial \widetilde{\mathbf{M}}_2} \cdot \widetilde{\mathbf{M}}_2 + 2\frac{\partial W}{\partial \widetilde{\mathbf{M}}_1} : (\widetilde{\mathbf{M}}_1 \otimes \widetilde{\mathbf{M}}_1) + 2\frac{\partial W}{\partial \widetilde{\mathbf{M}}_2} : (\widetilde{\mathbf{M}}_2 \otimes \widetilde{\mathbf{M}}_2). \tag{B.6}$$

- Summation of the first three terms ($W_{,j} = \partial W / \partial I_j$)

$$\begin{aligned} \mathbf{C}_\mathrm{e} \cdot \frac{\partial W}{\partial \mathbf{C}_\mathrm{e}} &= W_{,1}\mathbf{C}_\mathrm{e} + W_{,2}(I_1\mathbf{C}_\mathrm{e} - \mathbf{C}_\mathrm{e}^2) + W_{,3}I_3\mathbf{1} + W_{,4}\mathbf{C}_\mathrm{e} \cdot \widetilde{\mathbf{M}}_1 + W_{,5}\left(\mathbf{C}_\mathrm{e}^2 \cdot \widetilde{\mathbf{M}}_1 + \mathbf{C}_\mathrm{e} \cdot \widetilde{\mathbf{M}}_1 \cdot \mathbf{C}_\mathrm{e}\right) \\ &\quad + W_{,6}\mathbf{C}_\mathrm{e} \cdot \widetilde{\mathbf{M}}_2 + W_{,7}\left(\mathbf{C}_\mathrm{e}^2 \cdot \widetilde{\mathbf{M}}_2 + \mathbf{C}_\mathrm{e} \cdot \widetilde{\mathbf{M}}_2 \cdot \mathbf{C}_\mathrm{e}\right), \end{aligned} \tag{B.7}$$

$$-\frac{\partial W}{\partial \widetilde{\mathbf{M}}_1} \cdot \widetilde{\mathbf{M}}_1 = -W_{,4}\mathbf{C}_\mathrm{e} \cdot \widetilde{\mathbf{M}}_1 - W_{,5}\mathbf{C}_\mathrm{e}^2 \cdot \widetilde{\mathbf{M}}_1, \tag{B.8}$$

$$-\frac{\partial W}{\partial \widetilde{\mathbf{M}}_2} \cdot \widetilde{\mathbf{M}}_2 = -W_{,6}\mathbf{C}_\mathrm{e} \cdot \widetilde{\mathbf{M}}_2 - W_{,7}\mathbf{C}_\mathrm{e}^2 \cdot \widetilde{\mathbf{M}}_2. \tag{B.9}$$

- Final result for $\boldsymbol{\Sigma}$ (symmetric tensor)

$$\begin{aligned} \boldsymbol{\Sigma} &= 2W_{,1}\mathbf{C}_\mathrm{e} + 2W_{,2}(I_1\mathbf{C}_\mathrm{e} - \mathbf{C}_\mathrm{e}^2) + 2W_{,3}I_3\mathbf{1} + 2W_{,5}\mathbf{C}_\mathrm{e} \cdot \widetilde{\mathbf{M}}_1 \cdot \mathbf{C}_\mathrm{e} + 2W_{,7}\mathbf{C}_\mathrm{e} \cdot \widetilde{\mathbf{M}}_2 \cdot \mathbf{C}_\mathrm{e} \\ &\quad + \frac{\partial W}{\partial \widetilde{\mathbf{M}}_1} : (\widetilde{\mathbf{M}}_1 \otimes \widetilde{\mathbf{M}}_1) + \frac{\partial W}{\partial \widetilde{\mathbf{M}}_2} : (\widetilde{\mathbf{M}}_2 \otimes \widetilde{\mathbf{M}}_2). \end{aligned} \tag{B.10}$$

- Intermediate result

$$\left(\frac{\partial W}{\partial \widetilde{\mathbf{M}}_i} : \widetilde{\mathbf{M}}_i\right)\widetilde{\mathbf{M}}_i = W_{,2i+2}I_{2i+2}\widetilde{\mathbf{M}}_i + W_{,2i+3}I_{2i+3}\widetilde{\mathbf{M}}_i. \tag{B.11}$$

- Alternative representation of $\boldsymbol{\Sigma}$

$$\begin{aligned} \boldsymbol{\Sigma} &= 2W_{,1}\mathbf{C}_\mathrm{e} + 2W_{,2}(I_1\mathbf{C}_\mathrm{e} - \mathbf{C}_\mathrm{e}^2) + 2W_{,3}I_3\mathbf{1} + 2W_{,4}I_4\widetilde{\mathbf{M}}_1 + 2W_{,5}(I_5\widetilde{\mathbf{M}}_1 + \mathbf{C}_\mathrm{e} \cdot \widetilde{\mathbf{M}}_1 \cdot \mathbf{C}_\mathrm{e}) + 2W_{,6}I_6\widetilde{\mathbf{M}}_2 \\ &\quad + 2W_{,7}(I_7\widetilde{\mathbf{M}}_2 + \mathbf{C}_\mathrm{e} \cdot \widetilde{\mathbf{M}}_2 \cdot \mathbf{C}_\mathrm{e}). \end{aligned} \tag{B.12}$$

Appendix C

The purpose of this appendix is to show in which way the expression $\boldsymbol{\tau} : \mathbf{m}_i$ can be represented in terms of the stress tensor $\boldsymbol{\Sigma}$.

- Alternative representation of $\boldsymbol{\tau}_{\text{iso}} : \mathbf{m}_i$

$$\boldsymbol{\tau}_{\text{iso}} : \mathbf{m}_i = \text{tr}\left[2\mathbf{F}_{\text{e}} \cdot \left(\frac{\partial W}{\partial \mathbf{C}_{\text{e}}}\right)_{\text{iso}} \cdot \mathbf{F}_{\text{e}}^{\text{T}} \cdot \mathbf{F}_{\text{e}} \cdot \widetilde{\mathbf{M}}_i \cdot \mathbf{F}_{\text{e}}^{\text{T}} \frac{1}{I_{2i+2}}\right] = \text{tr}\left[\mathbf{C}_{\text{e}} \cdot \left(\frac{\partial W}{\partial \mathbf{C}_{\text{e}}}\right)_{\text{iso}} \cdot (\mathbf{C}_{\text{e}} \cdot \widetilde{\mathbf{M}}_i) \frac{1}{I_{2i+2}}\right]$$
$$= \boldsymbol{\Sigma}_{\text{iso}} : \text{sym}(\widetilde{\mathbf{M}}_i \cdot \mathbf{C}_{\text{e}}) \frac{1}{I_{2i+2}}. \tag{C.1}$$

- Alternative representation of $\boldsymbol{\tau}_{\text{ani}\,i} : \mathbf{m}_i$

$$\boldsymbol{\tau}_{\text{ani}\,i} : \mathbf{m}_i = \text{tr}[2W_{,2i+2}\overline{\mathbf{m}}_i + 2W_{,2i+3}(\mathbf{b}_{\text{e}} \cdot \overline{\mathbf{m}}_i + \overline{\mathbf{m}}_i \cdot \mathbf{b}_{\text{e}})] \cdot \mathbf{m}_i$$
$$= \text{tr}[2W_{,2i+2}\mathbf{m}_i I_{2i+2} + 2W_{2i+3}(\mathbf{b}_{\text{e}} \cdot \mathbf{m}_i + \mathbf{m}_i \cdot \mathbf{b}_{\text{e}})I_{2i+2}] = 2W_{,2i+2}I_{2i+2} + 4W_{,2i+3}I_{2i+3}, \tag{C.2}$$

$$\boldsymbol{\Sigma}_{\text{ani}\,i} : \text{sym}(\widetilde{\mathbf{M}}_i \cdot \mathbf{C}_{\text{e}}) \frac{1}{I_{2i+2}} = 2W_{,2i+2}I_{2i+2}\widetilde{\mathbf{M}}_i : (\widetilde{\mathbf{M}}_i \cdot \mathbf{C}_{\text{e}}) \frac{1}{I_{2i+2}}$$
$$+ 2W_{,2i+3}(I_{2i+3}\widetilde{\mathbf{M}}_i + \mathbf{C}_{\text{e}} \cdot \widetilde{\mathbf{M}}_i \cdot \mathbf{C}_{\text{e}}) : (\widetilde{\mathbf{M}}_i \cdot \mathbf{C}_{\text{e}}) \frac{1}{I_{2i+2}}. \tag{C.3}$$

- Intermediate results

$$\widetilde{\mathbf{M}}_i : (\widetilde{\mathbf{M}}_i \cdot \mathbf{C}_{\text{e}}) = I_{2i+2}, \tag{C.4}$$

$$(\mathbf{C}_{\text{e}} \cdot \widetilde{\mathbf{M}}_i \cdot \mathbf{C}_{\text{e}}) : (\widetilde{\mathbf{M}}_i \cdot \mathbf{C}_{\text{e}}) = \text{tr}(\mathbf{b}_{\text{e}} \cdot \mathbf{m}_i) I_{2i+2}^2 = I_{2i+3}I_{2i+2}. \tag{C.5}$$

- Final result

$$\boxed{\boldsymbol{\Sigma}_{\text{ani}\,i} : \text{sym}(\widetilde{\mathbf{M}}_i \cdot \mathbf{C}_{\text{e}}) \frac{1}{I_{2i+2}} = 2W_{,2i+2}I_{2i+2} + 4W_{,2i+3}I_{2i+3} = \boldsymbol{\tau}_{\text{ani}\,i} : \mathbf{m}_i.} \tag{C.6}$$

- Alternative representation of $\boldsymbol{\tau}_{\text{ani}\,2} : \mathbf{m}_1$

$$\boldsymbol{\tau}_{\text{ani}\,2} : \mathbf{m}_1 = \text{tr}[2W_{,6}\mathbf{m}_2 + 2W_{,7}(\mathbf{b}_{\text{e}} \cdot \mathbf{m}_2 + \mathbf{m}_2 \cdot \mathbf{b}_{\text{e}})] \cdot \mathbf{m}_1 I_6 = 2W_{,6}I_6\mathbf{m}_2$$
$$: \mathbf{m}_1 + 2W_{,7}I_6\,\text{tr}[\mathbf{b}_{\text{e}} \cdot \mathbf{m}_2 \cdot \mathbf{m}_1 + \mathbf{m}_1 \cdot \mathbf{m}_2 \cdot \mathbf{b}_{\text{e}}], \tag{C.7}$$

$$\boldsymbol{\Sigma}_{\text{ani}\,2} : \text{sym}(\widetilde{\mathbf{M}}_1 \cdot \mathbf{C}_{\text{e}}) \frac{1}{I_4} = 2W_{,6}I_6\widetilde{\mathbf{M}}_2 : (\widetilde{\mathbf{M}}_1 \cdot \mathbf{C}_{\text{e}}) \frac{1}{I_4} + 2W_{,7}(I_7\widetilde{\mathbf{M}}_2 + \mathbf{C}_{\text{e}} \cdot \widetilde{\mathbf{M}}_2 \cdot \mathbf{C}_{\text{e}}) : (\widetilde{\mathbf{M}}_1 \cdot \mathbf{C}_{\text{e}}) \frac{1}{I_4}. \tag{C.8}$$

- Intermediate results

$$\widetilde{\mathbf{M}}_2 : (\widetilde{\mathbf{M}}_1 \cdot \mathbf{C}_{\text{e}}) = \text{tr}\left(\mathbf{b}_{\text{e}}^{-1} \cdot \mathbf{m}_2 \cdot \mathbf{m}_1\right) I_4 I_6, \tag{C.9}$$

$$(\mathbf{C}_{\text{e}} \cdot \widetilde{\mathbf{M}}_2 \cdot \mathbf{C}_{\text{e}}) : (\widetilde{\mathbf{M}}_1 \cdot \mathbf{C}_{\text{e}}) = \text{tr}(\mathbf{b}_{\text{e}} \cdot \mathbf{m}_2 \cdot \mathbf{m}_1) I_4 I_6. \tag{C.10}$$

- Final result

$$\boxed{\boldsymbol{\Sigma}_{\text{ani}\,2} : \text{sym}(\widetilde{\mathbf{M}}_1 \cdot \mathbf{C}_{\text{e}}) \frac{1}{I_4} \neq \boldsymbol{\tau}_{\text{ani}\,2} : \mathbf{m}_1.} \tag{C.11}$$

Appendix D

The purpose of this appendix is to prove the statement

$$\text{sign}(\boldsymbol{\tau} : \mathbf{m}_i) = \text{sign}\left(\boldsymbol{\Sigma} : \text{sym}(\mathbf{M}_i \cdot \mathbf{C}_{\text{e}}) \frac{1}{I_{2i+2}}\right). \tag{D.1}$$

Due to (20), this boils down to show

$$\operatorname{sign}\underbrace{(\boldsymbol{\tau}_{\text{ani}\,2} : \mathbf{m}_1)}_{E_\tau} = \operatorname{sign}\underbrace{\left(\boldsymbol{\Sigma}_{\text{ani}\,2} : \operatorname{sym}(\widetilde{\mathbf{M}}_1 \cdot \mathbf{C}_{\text{e}})\frac{1}{I_4}\right)}_{E_\Sigma}. \tag{D.2}$$

The expressions E_τ and E_Σ are in detail expressed as

$$\begin{aligned} E_\tau &= 2I_6\big(W_{,6}\operatorname{tr}(\mathbf{m}_2 \cdot \mathbf{m}_1) + W_{,7}\operatorname{tr}(\mathbf{b}_{\text{e}} \cdot \mathbf{m}_2 \cdot \mathbf{m}_1 + \mathbf{m}_1 \cdot \mathbf{m}_2 \cdot \mathbf{b}_{\text{e}})\big),\\ E_\Sigma &= 2I_6\big(W_{,6}\operatorname{tr}(\mathbf{b}_{\text{e}}^{-1} \cdot \mathbf{m}_2 \cdot \mathbf{m}_1) + W_{,7}I_7\operatorname{tr}(\mathbf{b}_{\text{e}}^{-1} \cdot \mathbf{m}_2 \cdot \mathbf{m}_1) + \operatorname{tr}(\mathbf{b}_{\text{e}} \cdot \mathbf{m}_2 \cdot \mathbf{m}_1)\big). \end{aligned} \tag{D.3}$$

Exploiting the assumption made at the end of Section 3.1, it can be guaranteed that the terms $W_{,6}$ and $W_{,7}$ are always positive. Thus, we have to prove that the expressions $\operatorname{tr}(\mathbf{A} \cdot \mathbf{m}_2 \cdot \mathbf{m}_1)$ with $\mathbf{A} = \mathbf{1}$, $\mathbf{A} = \mathbf{b}_{\text{e}}^{-1}$ or $\mathbf{A} = \mathbf{b}_{\text{e}}$ respectively, have always the same sign.

For this purpose, we use the spectral decomposition

$$\mathbf{A} = \sum_{J=1}^{3} A_J \boldsymbol{\varphi}_J \otimes \boldsymbol{\varphi}_J, \tag{D.4}$$

(A_J eigenvalues and $\boldsymbol{\varphi}_J$ eigenvectors of $\mathbf{A}$) and represent the vectors $\mathbf{n}_1$ and $\mathbf{n}_2$ in terms of the eigenvectors $\boldsymbol{\varphi}_I$ ($I = 1, 2, 3$):

$$\mathbf{n}_1 = \sum_{I=1}^{3} a_I \boldsymbol{\varphi}_I, \qquad \mathbf{n}_2 = \sum_{I=1}^{3} b_I \boldsymbol{\varphi}_I. \tag{D.5}$$

If two or three eigenvalues of $\mathbf{b}_{\text{e}}$ are equal, the eigenvectors are chosen such that the orthogonality $\boldsymbol{\varphi}_I \cdot \boldsymbol{\varphi}_J = \delta_{IJ}$ is fulfilled. The coefficients a_I and b_I remain undetermined. One obtains

$$\operatorname{tr}(\mathbf{A} \cdot \mathbf{m}_2 \cdot \mathbf{m}_1) = (\mathbf{n}_2 \cdot \mathbf{n}_1)(\mathbf{n}_2 \cdot \mathbf{A} \cdot \mathbf{n}_1) \tag{D.6}$$

and

$$\mathbf{n}_2 \cdot \mathbf{A} \cdot \mathbf{n}_1 = \sum_{I=1}^{3}\sum_{J=1}^{3} a_I b_J \boldsymbol{\varphi}_I \cdot \left(\sum_{K=1}^{3} A_K \boldsymbol{\varphi}_K \otimes \boldsymbol{\varphi}_K\right) \cdot \boldsymbol{\varphi}_J = \sum_{K=1}^{3} a_K b_K A_K. \tag{D.7}$$

Since $\mathbf{A}$ is positive definite, its eigenvalues A_K are always positive. The sign of $\mathbf{n}_2 \cdot \mathbf{A} \cdot \mathbf{n}_1$ does not depend on the fact whether we make the choice $\mathbf{A} = \mathbf{b}_{\text{e}}$, $\mathbf{A} = \mathbf{b}_{\text{e}}^{-1}$ or $\mathbf{A} = \mathbf{1}$. Taking into account further that the invariants I_j ($j = 1, \ldots, 7$) are positive, the latter result guarantees $\operatorname{sign} E_\tau = \operatorname{sign} E_\Sigma$.

References

Asaro, R., 1983. Micromechanics of crystals and polycrystals. Advances in Applied Mechanics 23, 1–115.

Bertram, A., 1992. Description of finite inelastic deformations. In: Benallal, A., Billardon, R., Marquis, D. (Eds.), Proceedings of MECAMAT '92, International Seminar on Multiaxial Plasticity. pp. 821–835.

Bertram, A., 1998. An alternative approach to finite plasticity based on material isomorphisms. International Journal of Plasticity 52, 353–374.

Boehler, J.P., 1977. On irreducible representations for isotropic functions. Zeitschrift für Angewandte Mathematik und Mechanik 57, 323–327.

Boehler, J.P., 1979. A simple derivation of representations for non-polynomial constitutive equations in some cases of anisotropy. Zeitschrift für Angewandte Mathematik und Mechanik 59, 157–167.

Bonet, J., Burton, A.J., 1998. A simple orthotropic, transversely isotropic hyperelastic constitutive equation for large strain computations. Computer Methods in Applied Mechanics and Engineering 162, 151–164.

Cuitino, A.M., Ortiz, M., 1992. Computational modeling of single crystals. Modelling and Simulation in Materials Science and Engineering 1, 225–263.

Gasser, T.C., Holzapfel, G.A., submitted for publication. A rate-independent elastoplastic constitutive model for fiber-reinforced composites at finite strains: continuum basis, algorithmic formulation and finite element implementation.

Hill, R., 1966. Generalized constitutive relations for incremental deformation of metal crystals by multislip. Journal of the Mechanics and Physics of Solids 14, 95–102.

Holzapfel, G.A., Eberlein, R., Wriggers, P., Weizsäcker, H.W., 1996. A new axisymmetrical membrane element for anisotropic, finite strain analysis of arteries. Communications in Numerical Methods in Engineering 12, 507–517.

Holzapfel, G.A., Schulze-Bauer, C.A.J., Stadler, M., 2000. Mechanics of angioplasty: wall, balloon and stent. In: Casey, J., Bao, G. (Eds.), Mechanics in Biology, AMD-vol. 242/BED-vol. 46. The American Society of Mechanical Engineers (ASME), New York, USA, pp. 141–156.

Liu, S., 1982. On representations of anisotropic invariants. International Journal of Engineering Science 20, 1099–1109.

Menzel, A., Steinmann, P., 2001. A theoretical and computational framework for anisotropic inelasticity. In: Proceedings (CD-ROM) of 2. European Conference on Computational Mechanics, Cracow, Poland.

Miehe, C., 1996. Exponential map algorithm for stress updates in anisotropic multiplicative elastoplasticity for single crystals. International Journal for Numerical Methods in Engineering 39, 3367–3390.

Ogden, R.W., 1984. Non-linear elastic deformations. Ellis Horwood, Chichester.

Reese, S., Küssner, M., Reddy, B.D., 1999. A new stabilization technique for finite elements in non-linear elasticity. International Journal for Numerical Methods in Engineering 44, 1617–1652.

Reese, S., Wriggers, P., Reddy, B.D., 2000. A new locking-free brick element technique for large deformation problems in elasticity. Computers & Structures 75, 291–304.

Reese, S., Raible, T., Wriggers, P., 2001. Finite element modelling of orthotropic material behaviour in pneumatic membranes. International Journal of Solids and Structures 38, 9525–9544.

Rice, J.R., 1971. Inelastic constitutive relations for solids: an internal-variable theory and its application to metal plasticity. Journal of the Mechanics and Physics of Solids 19, 433–455.

Rumpel, T., Schweizerhof, K., in press. Volume dependent pressure loading and its influence on the stability of structures. International Journal for Numerical Methods in Engineering.

Sansour, C., Kollmann, F.G., 2001. Anisotropic formulations for finite strain viscoplasticity, Applications to shells. In: Wall, W.A., Bletzinger, K.-U., Schweizerhof, K. (Eds.), Proceedings of Trends in Computational Structural Mechanics. CIMNE, Barcelona, Spain.

Schmidt, I., 2001. On plasticity and deformation induced anisotropy in metallic foams. In: Banhart, J., Ashby, M., Fleck, N. (Eds.), Proceedings of Cellular Metals and Metal Foaming Technology, MetFoam 2001. MIT Publishing Bremen, Germany.

Schweizerhof, K., Ramm, E., 1984. Displacement dependent pressure loads in nonlinear finite element analyses. Computers & Structures 18, 1099–1114.

Simo, J.C., Miehe, C., 1992. Associative coupled thermoplasticity at finite strains: formulation, numerical analysis and implementation. Computer Methods in Applied Mechanics and Engineering 98, 41–104.

Spencer, A.J.M., 2001. A theory of viscoplasticity for fabric-reinforced composites. Journal of the Mechanics and Physics of Solids 49, 2667–2687.

Svendsen, B., 1994. On the representation of constitutive relations using structure tensors. International Journal of Engineering Science 32, 1889–1892.

Svendsen, B., 1998. A thermodynamic formulation of finite-deformation elastoplasticity with hardening based on the concept of material isomorphism. International Journal of Plasticity 14, 473–488.

Svendsen, B., 2001. On the modelling of anisotropic elastic and inelastic material behaviour at large deformation. International Journal of Solids and Structures 38, 9579–9599.

Svendsen, B., Reese, S., submitted for publication. On the modelling of internal variables as structure tensors in anisotropic finite deformation inelasticity. International Journal of Plasticity.

Wang, C.C., Bloom, J., 1974. Material uniformity and inhomogeneity in anelastic bodies. Archive for Rational Mechanics and Analysis 53, 246.

Weiss, J.A., Maker, B.N., Govindjee, S., 1996. Finite element implementation of incompressible, transversely isotropic hyperelasticity. Computer Methods in Applied Mechanics and Engineering 135, 107–128.

Zhang, Q.-S., Rychlewski, J.M., 1990. Structural tensors for anisotropic solids. Archives of Mechanics 42, 267–277.